PB80-197809

A Two-Mode Free-Surface Numerical Model for the Three-Dimensional Time-Dependent Currents in Large Lakes

Case Western Reserve Univ.
Cleveland, OH

Prepared for

Environmental Research Lab.-Duluth, MN

May 80

U.S. Department of Commerce
National Technical Information Service
NTIS.

TECHNICAL REPORT DATA
(Please read Instructions on the reverse before completing)

1. REPORT NO.	2.	3. RECIPIENT'S ACCESSION NO.
EPA-600/3-80-047		

4. TITLE AND SUBTITLE	5. REPORT DATE
A Two-Mode Free-Surface Numerical Model for the Three-Dimensional Time-Dependent Currents in Large Lakes	May 1980 issuing date
	6. PERFORMING ORGANIZATION CODE
7. AUTHOR(S)	8. PERFORMING ORGANIZATION REPORT NO.
Y. Peter Sheng and Wilbert Lick	
9. PERFORMING ORGANIZATION NAME AND ADDRESS Department of Earth Sciences Case Western Reserve University 2040 Adelbert Road Cleveland, Ohio 44106	10. PROGRAM ELEMENT NO. 1BA769 11. CONTRACT/GRANT NO. R803704
12. SPONSORING AGENCY NAME AND ADDRESS Environmental Research Laboratory Office of Research and Development U.S. Environmental Protection Agency Duluth, Minnesota 55804	13. TYPE OF REPORT AND PERIOD COVERED Final 14. SPONSORING AGENCY CODE EPA/600/03

15. SUPPLEMENTARY NOTES

16. ABSTRACT

A two-mode, free-surface model based on vertically-stretched coordinates and a vertically-implicit scheme has been developed and applied to Lake Erie under non-stratified conditions. A brief description of the general equations and boundary conditions is first given. The detailed equations for a two-mode, free-surface model are then described. Finite-difference procedures including the finite - difference equations are listed in detail. The model is first applied to idealized basins and then to Lake Erie for two wind conditions; (1) a uniform wind suddenly imposed, and (2) an actual wind variable in both space and time. The results of the computations are compared with the results from a single-mode, free-surface model and from a rigid-lid model.

17. KEY WORDS AND DOCUMENT ANALYSIS

a. DESCRIPTORS	b. IDENTIFIERS/OPEN ENDED TERMS	c. COSATI Field/Group
Hydrodynamics Circulation Mathematical Models Lakes	Lake Current Models Lake Erie	08H

18. DISTRIBUTION STATEMENT	19. SECURITY CLASS *(This Report)*	21. NO. OF PAGES
RELEASE TO PUBLIC	UNCLASSIFIED	70
	20. SECURITY CLASS *(This page)*	22. PRICE
	UNCLASSIFIED	

EPA Form 2220-1 (Rev. 4-77) PREVIOUS EDITION IS OBSOLETE

* U.S. GOVERNMENT PRINTING OFFICE: 1980-657-146/5669

United States
Environmental Protection
Agency

Environmental Research
Laboratory
Duluth MN 55804

EPA-600/3-80-047
May 1980

Research and Development

PB80-197409

EPA

A Two-Mode Free-Surface Numerical Model for the Three-Dimensional Time-Dependent Currents in Large Lakes

REPRODUCED BY
NATIONAL TECHNICAL
INFORMATION SERVICE
U. S. DEPARTMENT OF COMMERCE
SPRINGFIELD, VA. 22161

RESEARCH REPORTING SERIES

Research reports of the Office of Research and Development, U.S. Environmental Protection Agency, have been grouped into nine series. These nine broad categories were established to facilitate further development and application of environmental technology. Elimination of traditional grouping was consciously planned to foster technology transfer and a maximum interface in related fields. The nine series are:

1. Environmental Health Effects Research
2. Environmental Protection Technology
3. Ecological Research
4. Environmental Monitoring
5. Socioeconomic Environmental Studies
6. Scientific and Technical Assessment Reports (STAR)
7. Interagency Energy-Environment Research and Development
8. "Special" Reports
9. Miscellaneous Reports

This report has been assigned to the ECOLOGICAL RESEARCH series. This series describes research on the effects of pollution on humans, plant and animal species, and materials. Problems are assessed for their long- and short-term influences. Investigations include formation, transport, and pathway studies to determine the fate of pollutants and their effects. This work provides the technical basis for setting standards to minimize undesirable changes in living organisms in the aquatic, terrestrial, and atmospheric environments.

This document is available to the public through the National Technical Information Service, Springfield, Virginia 22161.

EPA-600/3-80-047
May 1980

A TWO-MODE FREE-SURFACE NUMERICAL MODEL FOR THE THREE-DIMENSIONAL TIME-DEPENDENT CURRENTS IN LARGE LAKES

by

Y. Peter Sheng and Wilbert Lick

Case Western Reserve University
Cleveland, Ohio 44106

Grant No. R-803704

PROJECT OFFICER

David M. Dolan
Large Lakes Research Station
Environmental Research Laboratory-Duluth
Grosse Ile, Michigan 48138

ENVIRONMENTAL RESEARCH LABORATORY
OFFICE OF RESEARCH AND DEVELOPMENT
U.S. ENVIRONMENTAL PROTECTION AGENCY
DULUTH, MINNESOTA 55804

DISCLAIMER

This report has been reviewed by the Environmental Research Laboratory, U.S. Environmental Protection Agency, and approved for publication. Approval does not signify that the contents necessarily reflect the views and policies of the U.S. Environmental Protection Agency, nor does mention of trade names or commercial products constitute endorsement or recommendation for use.

FOREWORD

The present report is part of a series of reports on research concerned with understanding more thoroughly and being able to predict the transport and fate of contaminants in lakes. This transport and fate is a complex matter which involves physical, chemical, and biological processes, all of which need to be considered before the fate of contaminants can be predicted.

This work has emphasized (1) the transport of contaminants throughout the lake, especially in the near-shore, and (2) sediment-water interactions including the biochemical transformations in the sediments and the physical processes of sediment resuspension and deposition. Earlier work was concerned mainly with these processes in a thermally non-stratified lake. The later work has concentrated more on the significant processes in a stratified lake.

J. David Yount, Ph.D.
Deputy Director
Environmental Research Laboratory-Duluth

ABSTRACT

A two-mode, free-surface model based on vertically-stretched coordinates and a vertically-implicit scheme has been developed and applied to Lake Erie under non-stratified conditions. A brief description of the general equations and boundary conditions is first given. The detailed equations for a two-mode, free-surface model are then described. Finite-difference procedures including the finite-difference equations are listed in detail. The model is first applied to idealized basins and then to Lake Erie for two wind conditions: (1) a uniform wind suddenly imposed, and (2) an actual wind variable in both space and time. The results of the computations are compared with the results from a single-mode, free-surface model and from a rigid-lid model.

CONTENTS

Foreword

Abstract iii

Figures iv

Acknowledgments vi

1. Introduction viii

2. Conclusions and Recommendations 1

3. Equations and Boundary Conditions 3

4. General Description of Numerical Model 5

5. Applications to Idealized Basins 12

6. Applications to Lake Erie 20

References 26

Appendices 54

A. Derivation of the vertically stretched equations 57

B. An Implicit Scheme 60

FIGURES

Number		Page
3.1	Cartesian coordinates located at the nominal lake surface.....	6
4.1	Basic numerical grid structure.....	14
4.2	Schematics of computational procedure.....	19
5.1	A two-dimensional basin.....	21
5.2	Integrated current and near-bottom current, and vertical profile of horizontal currents at point 1 of Fig. 5.1.....	22
5.3	Integrated current and near-bottom current, and vertical profile of horizontal currents at point 2 of Fig. 5.1.....	23
5.4	Results in a constant-depth square basin.....	25
6.1	Lake Erie bottom topography.....	27
6.2	Numerical grid structure, locations of wind stations, water level gauges, and bottom topography of Western Lake Erie.....	28
6.3	Surface elevation computed by free-surface model as a function of time at three locations in Lake Erie.....	30
6.4	Horizontal velocities at a constant 0.1 and 0.5 depth from surface after 3 hours.....	31
6.5	Horizontal velocities at a constant 0.1 and 0.5 depth surface after 24 hours.....	33
6.6	Wind speed as a function of time - 4 weather stations - Western Basin, wind stresses at Toledo and Point Pelee.....	34
6.7	Comparison of surface elevation computed by free surface model with water level measurement at 5 gauges.....	35
6.8a	Horizontal velocities at 0.1 and 0.5 depth as a function of time at station 1 (near Toledo).....	36
6.8b	Horizontal velocities at 0.1 and 0.5 depth as function of time at station 2 (near Point Pelee).....	37

6.9 Horizontal velocities at constant 0.1 and 0.5 depth from surface at 0600 3/7/76..... 39

6.10 Horizontal velocities at constant 0.1 and 0.5 depth from surface at 1200 3/7/76..... 40

6.11 Horizontal velocities at constant 0.1 and 0.5 depth from surface at 0000 3/8/76..... 41

6.12 Horizontal velocities at constant 0.1 and 0.5 depth from surface at 1200 3/8/76..... 42

6.13 Large-scale eddy observed by ERTS-1 (LANDSAT-1) off the tip of Point Pelee on 3/14/73..... 43

6.14 Horizontal velocities at constant 0.1 and 0.5 depth from surface at 1200 3/8/76..... 44

6.15 Horizontal velocities at constant 0.1 and 0.5 depth from surface at 0000 3/9/76..... 45

6.16 Horizontal velocities at 0.1 and 0.5 depth as function of time at station 1 (near Toledo)..... 46

6.17 Horizontal velocities at 0.1 and 0.5 depth as function of time at station 2 (near Point Pelee)..... 47

6.18 Time-averaged currents over 3 14-hour periods and the 42-hour period starting 0000 3/7/76 station 1 (near Toledo)..... 49

6.19 Time-averaged currents over 3 14-hour periods and the 42-hour period starting 0000 3/7/76 station 2 (near Point Pelee)..... 50

6.20 Daily-averaged horizontal velocities at constant 0.1 depth from surface face on 3/7/76..... 51

6.21 Daily-averaged horizontal velocities at constant 0.1 depth from surface on 3/8/76..... 52

ACKNOWLEDGMENTS

The writers wish to acknowledge with appreciation the support of this project by the Environmental Protection Agency. Mr. Dave Dolan served as Grant Project Officer.

The National Aeronautics and Space Administration, through Dr. Richard Gedney, has given us considerable computer time for which we are grateful. Mr. Frank Molls of NASA gave us considerable computer programming assistance.

SECTION 1

INTRODUCTION

The need to quantitatively understand and assess the environmental impact of power plant discharges, sewage outfalls, dredged material disposals, and other contaminants has recently resulted in an increased effort to understand the hydrodynamics of large lakes. Although some of the most important aspects of wind-driven circulation in a large lake can be understood from the analytical models of Ekman (1923) and Welander (1957), a detailed investigation of the currents in realistic situations often dictates the need of numerical modeling.

In order to mathematically model and hence predict the dispersion and fate of substances introduced into lakes, it is essential to be able to accurately model the time-dependent currents in the lake. For accurate prediction of the entire velocity field, three-dimensional, time-dependent numerical models are often needed and numerous models of this type have been developed. Reviews by Cheng et al. (1976) and Lick (1976a,b) have discussed several of these three-dimensional models.

The simplest kind of three-dimensional model is the single-mode, free-surface model which solves the equations of motion and continuity equation with a single numerical time step. Such models are quite general and have been applied to large lakes by Freeman et al. (1972), Katz and Kizlauskaus (1973), Haq et al. (1974), Sheng (1975), and Sheng and Lick (1976). These models consume a large amount of computer time since the maximum allowable numerical time step is limited by the time it takes a surface gravity wave to travel between two adjacent horizontal grid points, a very severe limitation.

In order to improve the numerical efficiency of the single-mode, free-surface model, rigid-lid models have been formulated and applied to large lakes by Liggett (1969), Paul and Lick (1974, 1979), and Bennett (1977). In this type of model, it is assumed that the vertical velocity at the undisturbed location of the free-surface is zero. This eliminates the motions and time scales associated with surface gravity waves and hence allows much larger numerical time steps and reduced computational times.

Berdahl (1971) and Crowley (1969, 1970) compared the rigid-lid model and single-mode, free-surface models in idealized oceanic basins and found the results for Rossby waves predicted by the two models were very different, although the rigid-lid model required much less computational time. Sheng et al. (1978) compared the rigid-lid and free-surface models for Lake Erie. They found that, for relatively short time intervals and in shallow waters, significant differences between the results of the two models occur. The

long-term, time-averaged circulations computed by the two models agreed well in periods of strong winds and active seiching.

Simons (1972, 1974, 1975) developed a two-mode, free-surface model for Lake Ontario based on a four-layer lattice. In this type of model, the external variables, i.e., the free-surface elevation and vertically integrated currents, are treated separately from the internal, three-dimensional flow variables. The free-surface gravity waves no longer limit the internal-mode calculations and much larger time steps may be used for the internal mode calculations with greatly reduced overall computational times.

One shortcoming of such a multi-layered model is the lack of vertical resolution in the shallow parts of the basin. In order to have the same vertical resolution in both the shallow and deeper parts of the basin, vertically stretched coordinates (Philips 1957, Freeman et al. 1972), which result in an equal number of uniformly-spaced vertical grid points over the entire basin, can be used.

Since Lake Erie is the shallowest of the Great Lakes, the effects of vertical diffusion and bottom shear stress are more pronounced than in other Great Lakes. The numerical stability criterion associated with the vertical diffusion terms in the governing equations is also much more stringent. Vertically implicit schemes can be used to resolve this problem.

In the present study, a two-mode, free-surface model based on vertically-stretched coordinates and a vertically-implicit scheme has been developed and applied to Lake Erie under non-stratified conditions. In the following, a brief description of the general equations and boundary conditions is first given. The detailed equations for a two-mode, free-surface model in non-stratified situations are then described. Finite-difference procedures including the finite-difference equations are listed in detail. The model is first applied to idealized basins and then to Lake Erie for two wind conditions: (1) a uniform wind suddenly imposed, and (2) an actual wind variable in both space and time. The results of the computations are compared with the results from a single-mode, free-surface model and from a rigid-lid model.

SECTION 2

CONCLUSIONS AND RECOMMENDATIONS

In the present study, a two-mode, free-surface numerical model capable of realistically predicting currents in lakes under non-stratified conditions has been developed. Vertically stretched coordinates have been used so as to have the same vertical resolution in all parts of the basin. A vertically implicit scheme has been used to eliminate numerical instabilities because of the small vertical distances between grid points. The model is operational and calculations have been made for both idealized and realistic basins and wind conditions with specific applications to Lake Erie. The present report describes the general numerical procedure and presents representative results of the calculations.

This two-mode, free-surface model consumes considerably less computer time than does a single-mode, free-surface model. The present model requires more computer time than does a rigid-lid model but is superior to the rigid-lid model in that it does not eliminate currents associated with free-surface oscillations.

In a previous report (Lick, 1976a), a survey of numerical models of lake currents was given and several recommendations on further work were made. These recommendations are presently being implemented and are still valid. In particular, it is suggested that a great deal of numerical experimentation be done using these models in order to: (1) Understand the general characteristics of flows in lakes, especially in the near-shore under stratified conditions, e.g., upwelling and mass flux through the thermocline; (2) Calculate details of specific flows and verify these by means of field observations, again especially in the nearshore. A combination of field observations, numerical experiments, and laboratory work needs to be done to determine more accurately the magnitude and functional dependences of the vertical and horizontal eddy diffusion coefficients, the wind stress-wind velocity relation, the wind factor ratio, and the bottom stress.

Hydrodynamic models are becoming quite detailed. Sufficient information on their use is becoming available so that confidence may be placed in their prediction. In particular, these models are sufficiently accurate so that they can be used as bases for models of sediment resuspension and transport, contaminant dispersion during dredging, phytoplankton and zooplankton growth, community succession, etc. and should be so used. The present hydrodynamic model, along with a wave-hindcasting model, has been used by the present authors in a study of the resuspension, deposition, and transport of sediments in the Western Basin of Lake Erie (Sheng and Lick, 1977b).

Hydrodynamic models generally have not considered the effects of waves, effects which become increasingly important as the depth of water decreases. For an adequate understanding of the dispersion of contaminants in these shallow, near-shore regions, further work needs to be done on the effects of waves. The direct effects of waves in causing contaminant transport and sediment resuspension and transport as well as the indirect effects in causing long-shore currents need to be investigated, made quantitative, applied to specific cases, and verified by means of field observations.

The hydrodynamics and dispersion of contaminants in a lake, particularly when the lake is thermally stratified, depend strongly on the turbulent production, dissipation, and transport processes. In the present analysis and in most analyses of the dynamics of a lake, the concept of an eddy coefficient has been used to describe turbulence. Recently, more sophisticated descriptions of turbulent transport processes have been developed (e.g. Kolmogorov, 1942; Harlow and Nakayama, 1967; Launder and Spalding, 1972; Donaldson, 1973; Lewellen, Teske, and Sheng, 1978). These models attempt to describe the dynamics of the turbulence more accurately by means of transport equations for certain turbulent properties of the flow. A comparative study of eddy-viscosity and these transport models as applied to lake dynamics would be useful. However, a major difficulty with the models, especially with regard to lake dynamics, is a deficiency in our knowledge of the sources of turbulence and how to parameterize the magnitude of these sources. This is the part of the investigation which needs to be emphasized.

SECTION 3

EQUATIONS AND BOUNDARY CONDITIONS

The basic equations used in the modeling of lake currents are the hydrodynamic equations of conservation of mass, momentum and energy plus an equation of state:

$$\frac{\partial u}{\partial x} + \frac{\partial v}{\partial y} + \frac{\partial w}{\partial z} = 0 \tag{3.1}$$

$$\frac{\partial u}{\partial t} = -\left(\frac{\partial u^2}{\partial x} + \frac{\partial uv}{\partial y} + \frac{\partial uw}{\partial z}\right) + fv - \frac{1}{\rho}\frac{\partial p}{\partial x} + \frac{\partial}{\partial x}\left(A_H \frac{\partial u}{\partial x}\right) + \frac{\partial}{\partial y}\left(A_H \frac{\partial u}{\partial y}\right) + \frac{\partial}{\partial z}\left(A_v \frac{\partial u}{\partial z}\right) \tag{3.2}$$

$$\frac{\partial v}{\partial t} = -\left(\frac{\partial uv}{\partial x} + \frac{\partial v^2}{\partial y} + \frac{\partial vw}{\partial z}\right) - fu - \frac{1}{\rho}\frac{\partial p}{\partial y} + \frac{\partial}{\partial x}\left(A_H \frac{\partial v}{\partial x}\right) + \frac{\partial}{\partial y}\left(A_H \frac{\partial v}{\partial y}\right) + \frac{\partial}{\partial y}\left(A_H \frac{\partial v}{\partial z}\right) \tag{3.3}$$

$$\frac{\partial p}{\partial z} = -\rho g \tag{3.4}$$

$$\frac{\partial T}{\partial t} = -\left(\frac{\partial uT}{\partial x} + \frac{\partial vT}{\partial y} + \frac{\partial wT}{\partial z}\right) + \frac{\partial}{\partial x}\left(K_H \frac{\partial T}{\partial x}\right) + \frac{\partial}{\partial y}\left(K_H \frac{\partial T}{\partial y}\right) + \frac{\partial}{\partial z}\left(K_V \frac{\partial T}{\partial z}\right) \tag{3.5}$$

$$\rho = \rho(T) \tag{3.6}$$

where x and y are the horizontal coordinates, z is the vertical coordinate pointing vertically upward to form a right-hand coordinate system with x and y (Figure 3.1), u,v, and w are the three-dimensional velocities in the x,y, and z directions, t is time, f is the Coriolis parameter equal to 10^{-4} sec^{-1}, g is the gravitational acceleration, p is the pressure, ρ is the density, T is the temperature, A_H and K_H are the horizontal eddy coefficients, and A_V and K_V are the vertical eddy coefficients.

Several assumptions are implicit in these equations. These are: (a) the pressure is assumed to vary hydrostatically in the z direction, (b) the Boussinesq approximation is valid, i.e., the effects of density variations are considered unimportant except in the bouyancy term, (c) eddy coefficients are used to account for turbulent diffusion effects, and (d) heat sources and sinks in the fluid are neglected.

At the free surface of the lake, the appropriate boundary conditions are: (a) The wind stress is specified,

$$A_V \frac{\partial u}{\partial z} = \tau_x^w \ , \ A_V \frac{\partial v}{\partial z} = \tau_y^w \tag{3.7}$$

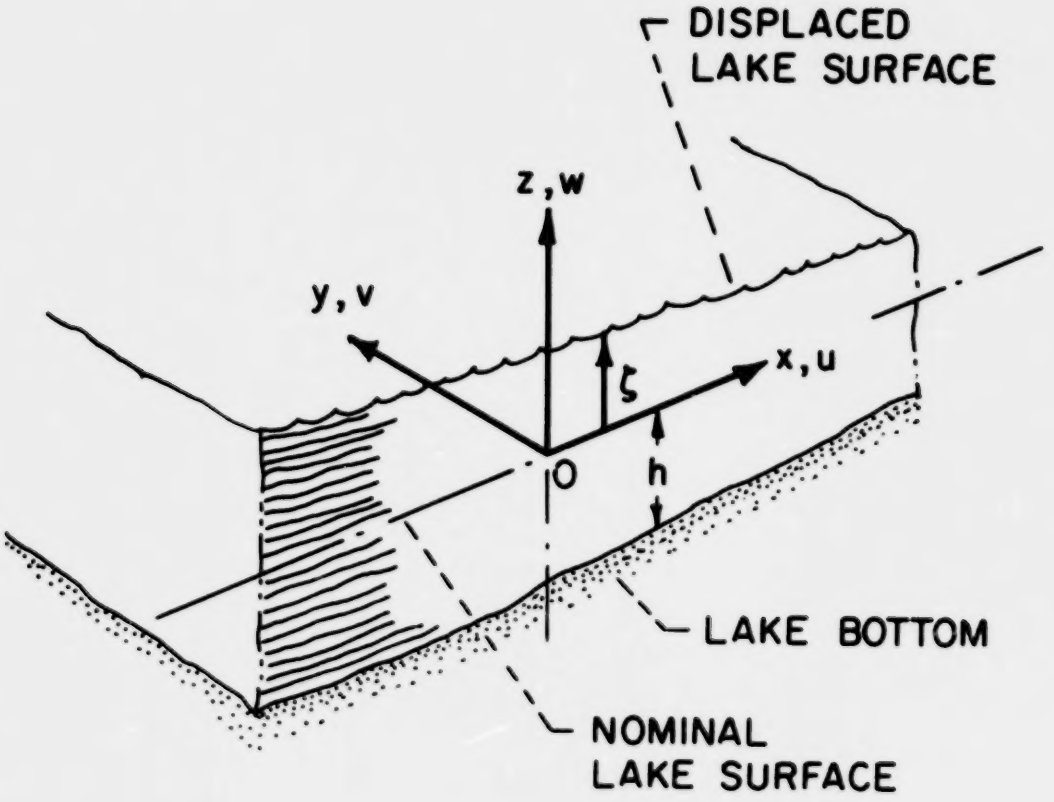

Figure 3.1 Cartesian coordinates located at the nominal lake surface.

where τ_x^w and τ_y^w are the wind stresses in the x and y directions respectively and are functions of the wind velocity; (b) the kinematic condition is satisfied,

$$w = \frac{\partial \zeta}{\partial t} + u\frac{\partial \zeta}{\partial x} + v\frac{\partial \zeta}{\partial y} \tag{3.8}$$

where ζ is the elevation of the free-surface; (c) The dynamic condition is satisfied,

$$p = p_a \tag{3.9}$$

where p_a is the atmospheric pressure; and (d) The heat flux is specified,

$$K_V \frac{\partial T}{\partial z} = q_s = \tilde{h}\ (T-T_e) \tag{3.10}$$

where T_e is the equilibrium air temperature at which the surface heat flux is zero and $\tilde{h}$ is the surface heat transfer coefficient.

At the bottom of the lake, the boundary conditions are: (a) a no-slip or zero-flow condition is assumed or it is assumed that:

$$\underline{\tau}^B = \rho C_d\ V_B\ \underline{V_B} \tag{3.11}$$

where $\underline{\tau}^B$ is the bottom shear stress vector, ρ is the water density, C_d is the skin-fraction coefficient, V_B is the magnitude of the bottom current while $\underline{V_B}$ is the bottom current vector; and (b) the heat flux or temperature is specified,

$$K_V \frac{\partial T}{\partial z} = q_B \text{ or } T = T_B \tag{3.12}$$

It is convenient to write the above system of equations and boundary conditions in non-dimensional form by defining the following non-dimensional quantities:

$$(u^*, v^*, w^*) = (u, v, wL/H) \ / \ U_r$$

$$(x^*, y^*, z^*) = (x, y, zL/H) \ / \ L$$

$$(\tau_x^*, \tau_y^*) = (\tau_x^w, \tau_y^w) \ / \ \rho(A_v)_r U_r$$

$$t^* = tf \ , \ p^* = p/\rho_v U_v f L$$

$$\rho^* = \rho/\rho_r, \ T^* = (T-T_r)/T_r, \ \zeta^* = g\zeta/fU_r L$$

$$A_H^* = A_H/(A_H)_r \ , \ A_v^* = A_v/(A_v)_r$$

$$K_H^* = K_H/(K_H)_r \ , \ K_v^* = K_v/(K_v)_r$$

where quantities with subscript r are reference quantities, and H and L are vertical and horizontal length scales.

Suppressing the asterisk (*) for clarity, the non-dimensional governing equations become:

$$\frac{\partial u}{\partial x} + \frac{\partial u}{\partial y} + \frac{\partial w}{\partial z} = 0 \tag{3.13}$$

$$\frac{\partial u}{\partial t} = R_B\left(\frac{\partial u^2}{\partial x} + \frac{\partial uv}{\partial y} + \frac{\partial uw}{\partial z}\right) + v - \frac{\partial p}{\partial x} + E_H\left[\frac{\partial}{\partial x}\left(A_H\frac{\partial u}{\partial x}\right) + \frac{\partial}{\partial y}\left(A_H\frac{\partial u}{\partial y}\right)\right] + E_V\frac{\partial}{\partial z}\left(A_V\frac{\partial u}{\partial z}\right) \tag{3.14}$$

$$\frac{\partial v}{\partial t} = -R_B\left(\frac{\partial uv}{\partial x} + \frac{\partial v^2}{\partial y} + \frac{\partial vw}{\partial z}\right) - u - \frac{\partial p}{\partial y} + E_H\left[\frac{\partial}{\partial x}\left(A_H\frac{\partial v}{\partial x}\right) + \frac{\partial}{\partial y}\left(A_H\frac{\partial v}{\partial y}\right)\right] + E_V\frac{\partial}{\partial z}\left(A_V\frac{\partial v}{\partial z}\right) \tag{3.15}$$

$$\frac{\partial p}{\partial z} = -\rho\, R_B/Fr^2 \tag{3.16}$$

$$\frac{\partial T}{\partial t} = -R_B\left(\frac{\partial uT}{\partial x} + \frac{\partial vT}{\partial y} + \frac{\partial wT}{\partial z}\right) + \frac{R_B}{Pe_H}\left[\frac{\partial}{\partial x}\left(K_H\frac{\partial T}{\partial x}\right) + \frac{\partial}{\partial y}\left(K_H\frac{\partial T}{\partial y}\right)\right] + \frac{R_B}{Pe_v}\frac{L}{H}\frac{\partial}{\partial z}\left(K_v\frac{\partial T}{\partial z}\right) \tag{3.17}$$

$$\rho = \rho(T) \tag{3.18}$$

where R_B = Rossby number = U_r/fL, E_H =horizontal Ekman number = $(A_H)_r/fL^2$, E_v = vertical Edman number = $(A_{Vr})/fH^2$, Fr = Froude number = $U_r/(gh)^{1/2}$, Pe_H = horizontal Peclet number = $U_vL/(K_{Hr})$, and Pe_v = vertical Peclet number = $U_rH/(K_v)_r$.

It is convenient to transform the equations from an x, y, z coordinate system to a vertically-stretched x, y, σ coordinate system where

$$\sigma = z/h(x,y) \tag{3.19}$$

where h(x,y) is the local depth of the lake. With this transformation and a uniform σ grid spacing, the number of grid points in the shallow areas of the lake is the same as in the deeper areas. Hence there is no loss of accuracy in the computations due to lack of vertical resolution. Freeman et al. (1972) used this method for investigating the circulation in Lake Huron. The equations resulting from this coordinate stretching are similar to the sigma equations derived by Phillips (1957).

The details of the derivation of the stretched equations are developed in Appendix A. The final set of non-dimensional equations are:

Continuity

$$\frac{\partial(hu)}{\partial x} + \frac{\partial(hv)}{\partial y} + h\frac{\partial \omega}{\partial \sigma} = 0 \tag{3.20}$$

x-momentum

$$\frac{\partial u}{\partial t} = -\frac{R_B}{h}\left[\frac{\partial(huv)}{\partial x} + \frac{\partial(huv)}{\partial y} + \frac{\partial(\omega u)}{\partial \sigma}\right] + v - \frac{\partial \zeta}{\partial x} - a_x +$$

$$\frac{E_H}{h}\left[\frac{\partial}{\partial x}\left(h\frac{\partial v}{\partial x}\right)+\frac{\partial}{\partial y}\left(h\frac{\partial v}{\partial y}\right)+\text{H.O.T.}\right]+\frac{E_V}{h^2}\frac{\partial}{\partial\sigma}\left(A_v\frac{\partial v}{\partial\sigma}\right) \tag{3.21}$$

y-momentum

$$\frac{\partial v}{\partial t} = -\frac{R_B}{h}\left[\frac{\partial(huv)}{\partial x}+\frac{\partial(hv^2)}{\partial y}+h\frac{\partial(\omega v)}{\partial\sigma}\right]-u-\frac{\partial\zeta}{\partial y}-a_y$$

$$\frac{E_H}{h}\left[\frac{\partial}{\partial x}\left(h\frac{\partial v}{\partial x}\right)+\frac{\partial}{\partial y}\left(h\frac{\partial v}{\partial y}\right)+\text{H.O.T.}\right]+\frac{E_V}{h^2}\frac{\partial}{\partial\sigma}\left(A_v\frac{\partial v}{\partial\sigma}\right) \tag{3.22}$$

Hydrostatic

$$\frac{\partial p}{\partial\sigma} = -\rho h\, R_B/Fr^2 \tag{3.23}$$

Energy

$$\frac{\partial T}{\partial t} = -\frac{R_B}{h}\left[\frac{\partial(huT)}{\partial x}+\frac{\partial(hvT)}{\partial y}+h\frac{\partial(\omega T)}{\partial\sigma}\right]+\frac{R_B}{Pe_H h}\left[\frac{\partial}{\partial x}\left(h\frac{\partial T}{\partial x}\right)+\frac{\partial}{\partial y}\left(h\frac{\partial T}{\partial y}\right)+\text{H.O.T.}\right]$$
$$+\frac{R_B L}{Pe_V H h^2}\frac{\partial}{\partial\sigma}\left(K_v\frac{\partial T}{\partial\sigma}\right) \tag{3.24}$$

Equation of state

$$\rho = \rho(T) \tag{3.25}$$

where a_x and a_y are defined as:

$$a_x = \frac{R_B}{Fr^2}\left[\int_\sigma^0 \frac{\partial\rho}{\partial x}\,d\sigma+\frac{\partial h}{\partial x}\left(\int_\sigma^0 \rho d\sigma+\sigma\rho\right)\right] \tag{3.26}$$

$$a_y = \frac{R_B}{Fr^2}\left[\int_\sigma^0 \frac{\partial\rho}{\partial y}\,d\sigma+\frac{\partial h}{\partial y}\left(\int_\sigma^0 \rho d\sigma+\sigma\rho\right)\right] \tag{3.27}$$

and where

$$\omega = \frac{w}{h}-\frac{\sigma}{h}\left(u\frac{\partial h}{\partial x}+v\frac{\partial h}{\partial y}\right) \tag{3.28}$$

The higher order terms (H.O.T.) in the horizontal diffusion terms contain bottom slopes and/or their products and hence are generally small compared to the listed leading terms when $H/L \ll 1$. It should be noted that in deriving Eqs. (3.21) and (3.22), the vertically-integrated form of the hydrostatic equation was substituted into the x- and y- momentum equations (Appendix A). Horizontal eddy coefficients were assumed to be independent of space and time and hence $A_H = 1$ and $K_H = 1$. In general, the vertical eddy coefficient is a function of the wind, local depth, and vertical temperature gradient. The following general form has been used by several authors (Munk and Anderson, 1948; Sundaram and Rehm, 1970):

$$A_v = A_{vo}\,(1+\sigma_1\,Ri)^m \tag{3.29}$$

$$K_v = K_{vo} (1 + \sigma_2 \, Ri)^n \tag{3.30}$$

where A_{vo} and K_{vo} are the eddy coefficients in the absence of any thermal stratification, σ_1, σ_2, m, and n are empirically determined constants, and Ri is the Richardson number which is the ratio of buoyancy and inertia forces:

$$Ri = \frac{-g\frac{\partial \rho}{\partial z}}{\rho\left(\frac{\partial \bar{u}}{\partial z}\right)^2} \tag{3.31}$$

where $\bar{u}$ is the mean horizontal velocity. Several linear or quadratic forms of the equation of state have been used by various authors (Paul and Lick, 1974; Simons, 1974).

The appropriate non-dimensional boundary conditions in the vertically-stretched coordinate system are as follows. Since the free-surface elevation is generally small compared to the water depth, it is generally valid to apply the free-surface boundary conditions at the undisturbed lake surface ($\sigma = 0$).

Surface, $\sigma = 0$:

$$\frac{\partial u}{\partial \sigma} = \frac{h\tau_x}{A_v} \, , \quad \frac{\partial v}{\partial \sigma} = \frac{h\tau_y}{A_v}$$

$$\frac{\partial T}{\partial \sigma} = \frac{H\tilde{h}h}{K_v} (T - T_e) \, , \quad \omega = \frac{1}{\beta h} \frac{\partial \zeta}{\partial t} \quad \text{where } \beta = gh/L^2 f^2$$

Bottom, $\sigma = -1$:

$$u = v = \omega = 0$$

$$\frac{1}{h} \frac{\partial T}{\partial \sigma} = q_B \quad \text{or} \quad T = T_B$$

River inflow or outflow:

$$u = u(x,y,\sigma)$$

$$v = v(x,y,\sigma)$$

$$T = T(x,y,\sigma)$$

Shore: $u = v = 0$

$$\frac{\partial T}{\partial n} = 0$$

Notice that the higher order terms which contain bottom slopes are neglected in the bottom boundary condition.

During time periods when thermal stratification in the lake is insignificant and hence the density and temperature are approximately uniform,

the energy equation and equation of state are decoupled from the momentum equations. The terms a_x and a_y in Eqs. (3.21) and (3.22) become zero. In Lake Erie, this constant density condition is approximately valid from late Fall to early Spring. For the shallow Western Basin of Lake Erie, this assumption is approximately valid throughout the entire year.

SECTION 4

GENERAL DESCRIPTION OF NUMERICAL MODEL

Basic Equations of the Two-Mode Model

As a first step in the development of a two-mode, free-surface model, a non-stratified lake is considered. The general procedure of the two-mode model remains basically unchanged when the effects of thermal stratification are included.

In single-mode, free-surface models for a non-stratified lake, Eqs. (3.20), (3.21), (3.22), (3.23) and associated boundary conditions are solved directly by finite-difference techniques. Due to the presence of free-surface gravity waves, the numerical time step is limited by the Courant-Frederick-Levy condition which, in dimensional form, is

$$\Delta t \leq \frac{\Delta x}{\sqrt{2gh_{max}}} \tag{4.1}$$

where Δx is the horizontal grid size, h_{max} is the maximum depth of the lake, and $\sqrt{gh_{max}}$ is the maximum speed of propagation of surface gravity waves. For Lake Erie, with a maximum depth of 61 m and Δx of 1km, the maximum allowable Δt is only 29 sec.

To alleviate this problem, a two-mode, free-surface model which treats the external and internal modes separately can be used. The external mode of the flow, i.e., the free-surface elevation and vertically-integrated currents, are calculated from the following vertically integrated continuity equation and equations of motion.

$$\frac{\partial \zeta}{\partial t} = -\beta\left(\frac{\partial U}{\partial x} + \frac{\partial V}{\partial y}\right) \tag{4.2}$$

$$\frac{\partial U}{\partial t} = -R_B\left[\frac{\partial}{\partial x}\left(\alpha_x \frac{U^2}{h}\right) + \frac{\partial}{\partial y}\left(\alpha_{xy}\frac{UV}{h}\right)\right] + V - h\frac{\partial \zeta}{\partial x} + E_H\left(\frac{\partial^2 U}{\partial x^2} + \frac{\partial^2 U}{\partial y^2}\right) + E_V(\tau_x^w - \tau_x^B) \tag{4.3}$$

$$\frac{\partial V}{\partial t} = -R_B\left[\frac{\partial}{\partial x}\left(\alpha_{xy}\frac{UV}{h}\right) + \frac{\partial}{\partial y}\left(\alpha_y \frac{V^2}{h}\right)\right] - U - h\frac{\partial \zeta}{\partial y} + E_H\left(\frac{\partial^2 V}{\partial x^2} + \frac{\partial^2 V}{\partial y^2}\right) + E_V(\tau_y^w - \tau_y^B) \tag{4.4}$$

where U and V are vertically-integrated velocities defined as

$U = \int_{-h}^{0} u\,dz = h\int_{-1}^{0} u\,d\sigma$, $V = \int_{-1}^{0} v\,dz = h\int_{-1}^{0} v\,d\sigma$, τ_x^B and τ_y^B are the components in the x and y directions of the bottom shear stresses in the σ-coordinate

system and are given by

$$\tau_x^B = \frac{1}{h}\left[1 + \frac{E_H}{E_V}\left\{\left(\frac{\partial h}{\partial x}\right)^2 + \left(\frac{\partial h}{\partial y}\right)^2\right\}\right]\left(\frac{\partial u}{\partial \sigma}\right)_{\sigma = -1}$$

$$\tau_y^B = \frac{1}{h}\left[1 + \frac{E_H}{E_V}\left\{\left(\frac{\partial h}{\partial x}\right)^2 + \left(\frac{\partial h}{\partial y}\right)^2\right\}\right]\left(\frac{\partial v}{\partial \sigma}\right)_{\sigma = -1}$$

and α_x, α_y and α_{xy} are defined as $\alpha_x = \int_{-1}^{0} \left(\frac{uh}{U}\right)^2 d\sigma$, $\alpha_y = \int_{-1}^{0} \left(\frac{vh}{V}\right)^2 d\sigma$,

and $\alpha_{xy} = \int_{-1}^{0} \left(\frac{uh}{U}\right)\left(\frac{vh}{V}\right) d\sigma$.

The internal mode is described by gradients in the vertical direction. The governing equations for the internal flow variables thus consist of the equations of motion and continuity equation in terms of differences between adjacent grid points in the vertical direction:

$$\frac{\partial(h\Delta u_k)}{\partial x} + \frac{\partial(h\Delta v_k)}{\partial y} + h\frac{\partial(\Delta \omega_k)}{\partial \sigma} = 0 \tag{4.5}$$

$$\frac{\partial(\Delta u_k)}{\partial t} = -\frac{R_B}{h}\left[\frac{\partial}{\partial x}\left[h\Delta(u_k^2)\right] + \frac{\partial}{\partial y}\left[h\Delta(u_k v_k)\right] + h\frac{\partial}{\partial \sigma}\left[\Delta(u_k \omega_k)\right]\right]$$
$$+ \Delta v_k + \frac{E_H}{h}\left[\frac{\partial}{\partial x}\left(h\frac{\partial(\Delta u_k)}{\partial x}\right) + \frac{\partial}{\partial y}\left(h\frac{\partial(\Delta u_k)}{\partial y}\right) + \frac{E_v}{h^2}\frac{\partial}{\partial \sigma}\left(A_v\frac{\partial(\Delta u_k)}{\partial \sigma}\right)\right] \tag{4.6}$$

$$\frac{\partial(\Delta v_k)}{\partial t} = -\frac{R_B}{h}\left[\frac{\partial}{\partial x}\left[h\Delta(u_k v_k)\right] + \frac{\partial}{\partial y}\left[h\Delta(v_k^2)\right] + h\frac{\partial}{\partial \sigma}\left[\Delta(v_k \omega_k)\right]\right]$$
$$-\Delta u_k + \frac{E_H}{h}\left[\frac{\partial}{\partial x}\left(h\frac{\partial(\Delta v_k)}{\partial x}\right) + \frac{\partial}{\partial y}\left(h\frac{\partial(\Delta u_k)}{\partial y}\right) + \frac{E_V}{h^2}\frac{\partial}{\partial \sigma}\left(A_v\frac{\partial(\Delta v_k)}{\partial \sigma}\right)\right] \tag{4.7}$$

where u_k, v_k, and ω_k are fluid velocities in the x, y, and σ directions at the k-th grid point in the vertical direction, k ranges from 1 near the bottom to $k = k_{max}$ near the surface, and $\Delta F_k = F_{k+1} - F$ is defined as the difference in the variable F between the $(k + 1)$-th and the k-th grid points. Higher order terms in the horizontal turbulence terms are listed in Appendix A.

In order to circumvent the non-linearity of the equations, a time-lagged approximation is introduced when integrating Eqs. (4.3), (4.4), (4.6) and (4.7) with respect to time, i.e., the non-linear terms are evaluated by means of values of u, v, and ω at the previous time interval.

Grid Structure

The basic grid structure is shown in Figure 4.1. The indices i, j, and k correspond respectively to x, y, and σ coordinates. In the staggered grid in the x-y plane, the variables u and U are calculated at the mid-points of the two boundaries parallel to the y-axis, v and V are calculated at the mid-

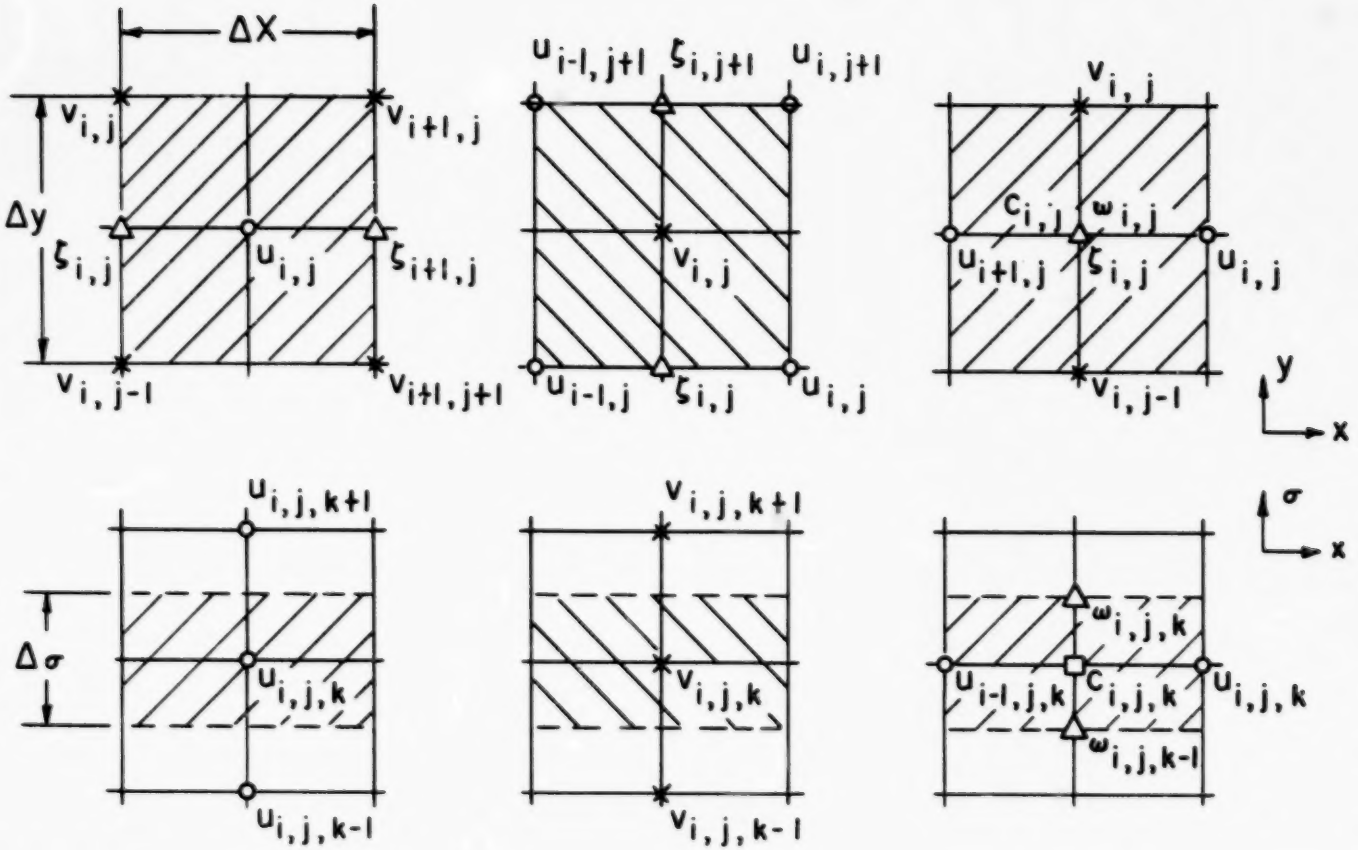

Figure 4.1 Basic numerical grid structure.

points of the two boundaries parallel to the x-axis, and ω and ζ are calculated at the center of the grid. In the σ direction, ω is calculated at full grid points and u and v are calculated at the mid-points. In the numerical calculation for an actual lake, the shoreline is fitted with a rectangular grid such that u equals zero or is determined by the river flow along a shoreline parallel to the y-axis and v equals zero or is determined by the river flow along a shoreline parallel to the x-axis.

The use of staggered grid avoids calculating all variables at all grid points and also greatly simplifies the evaluation of gradient terms in the finite difference equations. To evaluate variables at grid points where they are not defined, simple averaging is performed:

$$v_{u(i,j)} = \frac{1}{4}\left(v_{i,j} + v_{i,j-1} + v_{i+1,j} + v_{i+1,j-1}\right) \tag{4.8}$$

where u(i,j) indicates the grid point at which $u_{i,j}$ is evaluated. Details of evaluating the variables at various types of grid points can be found in Sheng (1975).

Finite Difference Equations

Various one and two-step methods were used to solve the external equations in a rectangular lake with constant depth or constant bottom slope. Based on extensive numerical experiments with these schemes, a two-step method similar to the Lax-Wendroff two-step method (Richtmeyer, 1967) was chosen for the numerical integration of Eqs. (4.2), (4.3) and (4.4). This scheme gives numerically-stable and accurate results and also does not have the time-splitting problem generally associated with the usual three-time-level schemes. It is convenient to write Eqs. (4.2), (4.3), and (4.4) as:

$$\frac{\partial U}{\partial t} = E(U,V,\zeta,u,\ldots) + V \tag{4.9}$$

$$\frac{\partial V}{\partial t} = F(U,V,\zeta,v,\ldots) - U \tag{4.10}$$

$$\frac{\partial \zeta}{\partial t} = G(U,V,\ldots) \tag{4.11}$$

where E and F represent the right-hand-sides of Eqs. (3.3) and (3.4) excluding the Coriolis term and G represents the right-hand-side of Eq. (3.2). These equations are solved in the following two steps. First, evaluate the variables at $t + \Delta t_e/2$ from the results at t and the previous internal time level, i.e.,

$$U^{n+1/2} = U^n + \frac{\Delta t_e}{2} E^* (U^n, V^n, \zeta^n, u^m, \ldots) + \frac{\Delta t_e}{2} V^n \tag{4.12}$$

$$V^{n+1/2} = V^n + \frac{\Delta t_e}{2} F^* (U^n, V^n, {}^n, v^m, \ldots) - \frac{\Delta t_e}{2} U^n \tag{4.13}$$

$$\zeta^{n+1/2} = \zeta^n + \frac{\Delta t_e}{2} G^* (U^{n+1/2}, V^{n+1/2}, \ldots) \tag{4.14}$$

Second, evaluate the variables at $t + \Delta t_e$ from the results at t, $t + \Delta t_e/2$,

and the previous internal time level, i.e.,

$$U^{n+1} = U^n + \Delta t_e\, E^* \,(U^{n+1/2}, V^{n+1/2}, \zeta^{n+1/2}, u^m, \ldots) + \Delta t_e V^n \tag{4.15}$$

$$V^{n+1} = V^n + \Delta t_e\, F^* \,(U^{n+1/2}, V^{n+1/2}, \zeta^{n+1/2}, v^m, \ldots) - \Delta t_e U^n \tag{4.16}$$

$$\zeta^{n+1} = \zeta^n + \Delta t_e\, G^* \,(U^{n+1}, V^{n+1}, \ldots) \tag{4.17}$$

where Δt_e indicates the external numerical time step (limited by Eq. (3.1), n and n + 1 are indices indicating the previous and present external time levels, m indicates the previous internal time level, and E*, F*, and G* are the finite-difference forms of E, F and G. Spatial derivatives are central differenced. For example, for $\frac{\partial \zeta}{\partial x}$ at the point u(i,j) where u is evaluated (see Figure 4.1), we have

$$\left(\frac{\partial \zeta}{\partial x}\right)_{u(i,j)} = \frac{\zeta_{i+1,j} - \zeta_{i,j}}{\Delta x} \tag{4.18}$$

$\left(\frac{\partial^2 U}{\partial x^2}\right)_{i,j}$ is evaluated by

$$\left(\frac{\partial^2 U}{\partial x^2}\right)_{i,j} = \frac{U_{i+1,j} - 2U_{i,j} + U_{i-1,j}}{(\Delta x)^2} \tag{4.19}$$

A rigorous analysis of the numerical stability of the above system of equations is extremely complicated, if not impossible. Instead, stability criteria for individual terms can be established and used as guidelines in choosing the proper Δt_e. It can be shown that for a deep lake the stability condition imposed by Eq. (4.1) is generally much more restrictive than those imposed by the horizontal turbulence or non-linear inertia terms.

Internal Mode

The numerical stability criterion associated with the vertical turbulent diffusion term can be studied by considering the one-dimensional heat equation in dimensionless form:

$$\frac{\partial u}{\partial t} = \frac{E_v}{h^2} \frac{\partial^2 u}{\partial \sigma^2} \tag{4.20}$$

The stability criterion for the forward-time, central-space or FTCS method for the finite-difference form of Eq. (4.20) is:

$$\Delta t \leq \frac{E_v}{2h^2 (\Delta \sigma)^2} \tag{4.21}$$

For conditions typical of Lake Erie, h = 10m, $A_v = 25 cm^2/sec$, $\Delta\sigma = 1/6$, and $\Delta t \leq 600$ sec. However, in the near-shore region where h is only 2m,

$\Delta t \leq 24$ sec. Hence the stability criterion (4.21) is much more restrictive than those associated with the other terms in the equations of motion. To remove the restriction (4.21), we tried three schemes: (1) Du-Fort Frankel, (2) Hopskotch, and (3) Implicit (see Appendix B). The implicit scheme was found to be unconditionally stable and also did not give any non-physical oscillations in the results as did the other two schemes. The implicit scheme is also relatively easy to implement even for the three-dimensional system and was therefore adopted for the present study. Applying the vertically implicit scheme to Eqs. (4.6) and (4.7), the difference equations are as follows:

$$(\Delta u_k)^{m+1} = (\Delta u_k)^m + \Delta t_i[(\text{Coriolis})^m + (\text{Horizontal Turbulence})^m + (\text{Vertical Turbulence})^{m+1} + (\text{Non-Linear Inertia})^m] \quad (4.22)$$

$$(\Delta v_k)^{m+1} = (\Delta v_k)^m + \Delta t_i[(\text{Coriolis})^m + (\text{Horizontal Turbulence})^m + (\text{Vertical Turbulence})^{m+1} + (\text{Non-Linear Inertia})^m] \quad (4.23)$$

where Δt_i indicates the internal numerical time step and m and m + 1 are indices indicating the previous and present internal time levels (t and t + Δt_i).

Although the horizontal eddy coefficient is much larger than the vertical eddy coefficient, the horizontal grid size is generally several orders of magnitude larger than the vertical grid size. Hence the stability limit imposed by the horizontal turbulence terms is generally not as restrictive as to warrant the use of an implicit scheme.

At every horizontal location i,j where u and v are calculated, there are k_{max} grid points in the σ direction and hence k_{max} -1 equations for Δu_k or Δv_k. In order to solve for the horizontal velocities at all k_{max} levels, two additional equations are provided from the external mode equations with the bottom stress terms treated implicitly:

$$U^{m+1} = U^{m+1-\Delta t_e/\Delta t_i} + \Delta t_e\ E^*\ (U^{m+1},\ldots) - \Delta t_e\ V^{m+1-\Delta t_e/\Delta t_i} \quad (4.24)$$

$$V^{m+1} = V^{m+1-\Delta t_e/\Delta t_i} + \Delta t_e\ F^*\ (V^{m+1},\ldots) + \Delta t_e\ U^{m+1-\Delta t_e/\Delta t_i} \quad (4.25)$$

The vertical velocity ω is computed from

$$\omega^{m+1}_{i,j,k} = \omega^{m+1}_{i,j,k-1} - \frac{1}{h\zeta_{(i,j)}}\left[\frac{\Delta\sigma}{\Delta x}\left(h_{u(i,j)}u^{m+1}_{i,j,k} - h_{u(i,j)}\ u^{m+1}_{i-1,j,k}\right)\right.$$
$$\left. + \frac{\Delta\sigma}{\Delta y}\left(h_{v(i,j)}v^{m+1}_{i,j,k} - h_{v(i,j-1)}\ v^{m+1}_{i,j-1,k}\right)\right] \quad (4.26)$$

and the surface elevation ζ can be calculated from

$$\zeta_{i,j}^{m+1} = \zeta^{m+1-\Delta t_e/\Delta t_i} - \Delta t_e \beta h \zeta_{(i,j)} \omega_{i,j,k_{max}}^{m+1} \tag{4.27}$$

Numerical Procedure

To maintain numerical stability, the numerical time step for the external mode calculation Δt_e is limited by Eq. (4.1), while the time step for the internal mode Δt_i is several times larger.

The computational procedure is schematically shown in Figure 4.2. At a typical time level, the three-dimensional velocities u,v,ω and the external variables U, V, ζ are known (from the previous computations or the given initial condition), and the bottom shear stress τ_B can be evaluated from the vertical profile of velocities. Subsequently, a relatively small time step Δt_e is used to integrate the vertically-integrated equations by explicit marching in time. Values of U, V, and ζ are evaluated from Eqs. (4.12) through (4.17) whereas the bottom stress in the momentum equations is not updated until after N - 1 steps, where $N = \Delta t_i/\Delta t_e$ and is an integer. The internal mode equations (4.22) and (4.23) are then integrated with a relatively large time step Δt_i while simultaneously integrating the vertically integrated momentum equation from $(N - 1)\Delta t_e$ to $N\Delta t_e$. For consistency, both the vertical diffusion terms in the internal equations and the bottom stress terms in the external equations are treated implicitly. The vertical velocity ω, surface elevation ζ, and bottom stress τ_B can then be calculated from the appropriate equations. This cyclic procedure is repeated until the computation is complete.

From formal analysis, the use of a vertically implicit scheme indicates unconditional numerical stability and hence the internal numerical time step is only limited by the convective terms. However, in a shallow lake, the bottom stress is quite significant compared to the wind stress and varies appreciably with time in transient situations. Hence the use of an internal time step Δt_i larger than the time scale associated with the variation of bottom stress, i.e., $\frac{H^2}{2A_v}$, would result in an oscillation of the solution leading to numerical instability. This additional constraint on the numerical time step is

$$t_i \leq \frac{h_{min}^2}{2A_v} \tag{4.28}$$

where h_{min} indicates the minimum depth of the basin.

Since Δt_e is proportional to Δx whereas Δt_i in a shallow lake is generally limited by Eq. (4.28) and hence independent of Δx, the external mode calculation generally takes proportionally less time in a coarser numerical grid relative to the internal mode calculation.

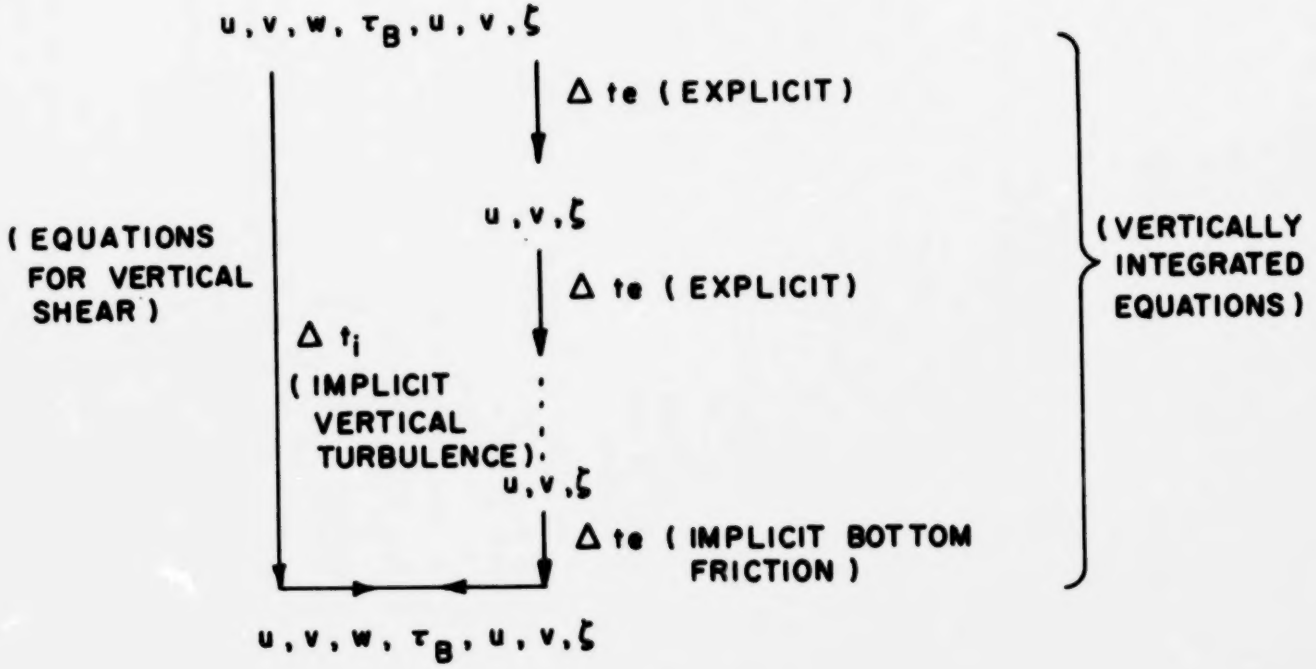
u, v, w, τB, u, v, ζ
Δ te (EXPLICIT)
u, v, ζ
Δ te (EXPLICIT)
Δ ti
(IMPLICIT VERTICAL TURBULENCE)
u, v, ζ
Δ te (IMPLICIT BOTTOM FRICTION)
u, v, w, τB, u, v, ζ
(EQUATIONS FOR VERTICAL SHEAR)
(VERTICALLY INTEGRATED EQUATIONS)

Figure 4.2. Schematics of computational procedure.

SECTION 5

APPLICATIONS TO IDEALIZED BASINS

A Two-Dimensional Basin

Extensive numerical experiments were carried out for a two-dimensional lake to test the performance of the two-mode hydrodynamic model. Some representative results are described here.

As shown in Figure 5.1, the two-dimensional lake represents a vertical cross-section of a three-dimensional lake. The basin was assumed to be 2 m deep at the shallow end with the depth increasing linearly to 30 m at the deep end over a width of 100 km. A uniform wind stress of 1 dyne/cm was assumed to be suddenly imposed at the surface and the flow variables were calculated for 48 hours. Representative results at two locations, one near the shallow shore and one near the deep shore, are shown in Figures 5.2 and 5.3.

At point 1 near the shallow shore, as shown in Figure 5.2, the time histories of the vertically integrated current and the horizontal current near the bottom are very similar. Both showed significant oscillation, with a distinct period of approximately 5 hours associated with the seiche oscillation in the basin. A steady state is approached in about 24 hours. The vertical profiles of horizontal velocities at several times are also shown in Figure 5.2 The results indicate that, due to the shallow depth, the effect of bottom friction is dominant during the transient stage. The use of a Δt_i greater than the vertical diffusion time of $\frac{h^2}{2A_v}$ = 4600 sec (based on h = 4.8 m and A_v = 25 cm/sec) resulted in oscillations in the solution. The results computed with Δt_i = 3600 sec = 1 hr and Δt_e = 600 sec = 10 min agree well with those computed with $\Delta t_i = \Delta t_e$ = 10 min.

At point 2 near the deep end, as shown in Figure 5.3, the vertically integrated current indicates a transient oscillation with a 5-hour period lasting for about 24 hours. However, the bottom current slowly increased with time with little oscillation. The effect of bottom friction is relatively less important at point 2 than at point 1.

A Constant-Depth Square Basin

As another example, flow in a square basin 50 km by 50 km with a depth of 10 m was studied. A uniform wind stress of 1 dyne/cm^2 in the x-direction was suddenly imposed. The vertical eddy viscosity was assumed to be 25 cm^2/sec, a typical value for Lake Erie under moderate wind conditions. The results are computed with Δx = 5 km, $\Delta\sigma$ = 1/6, Δt_e = 5 min and Δt_i = 1 hr.

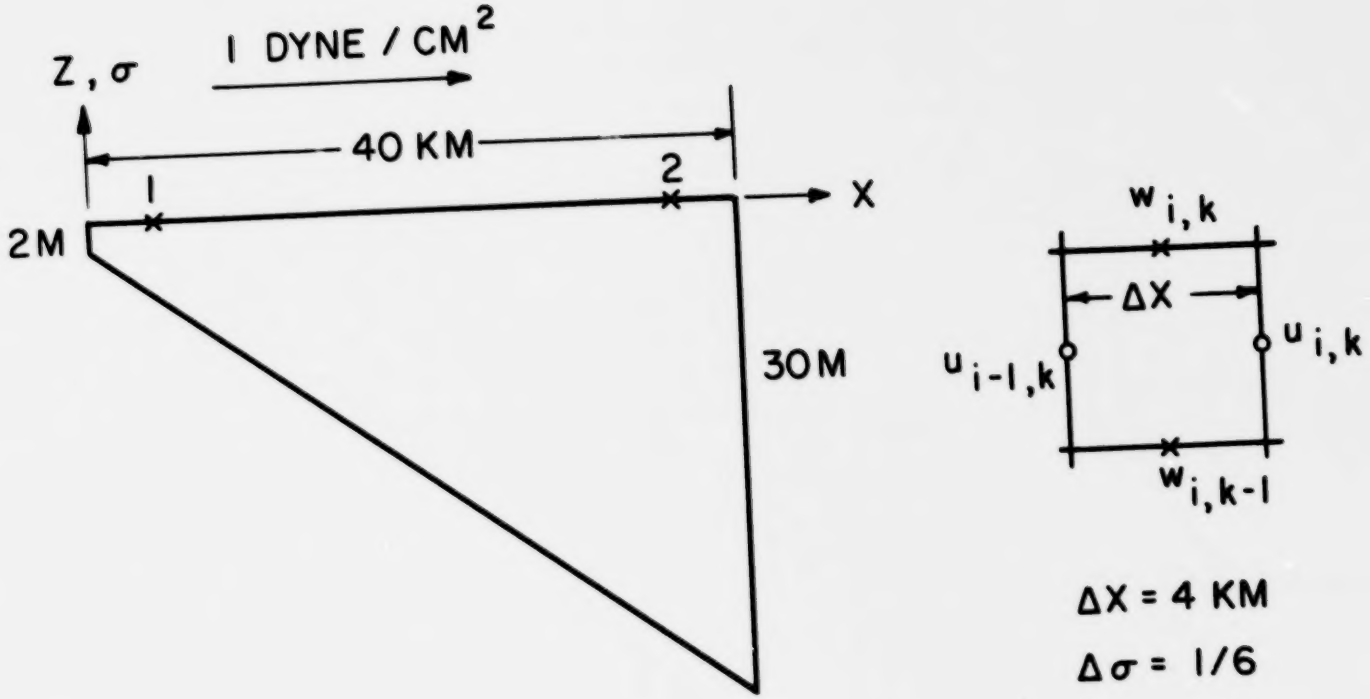

Figure 5.1 A Two-dimensional basin.

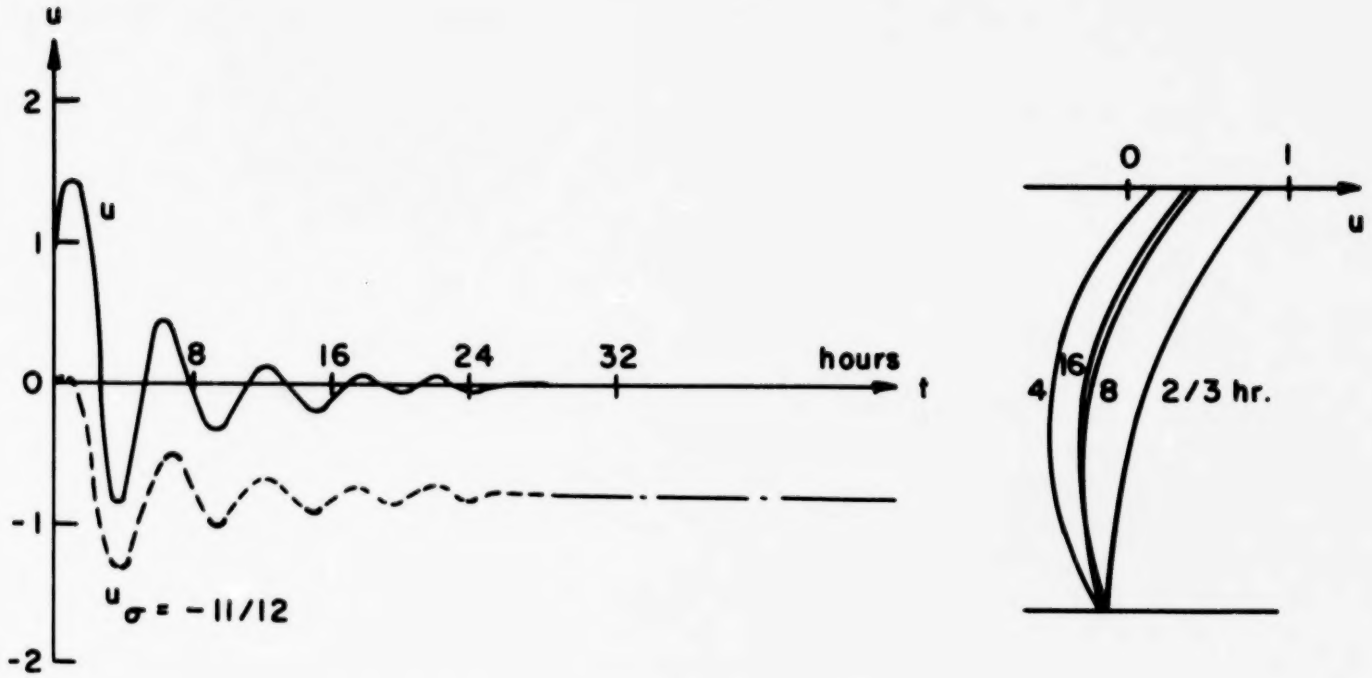

Figure 5.2. (a) Integrated current and near-bottom current, and
(b) Vertical profile of horizontal currents at point 1 of Fig. 5.1.

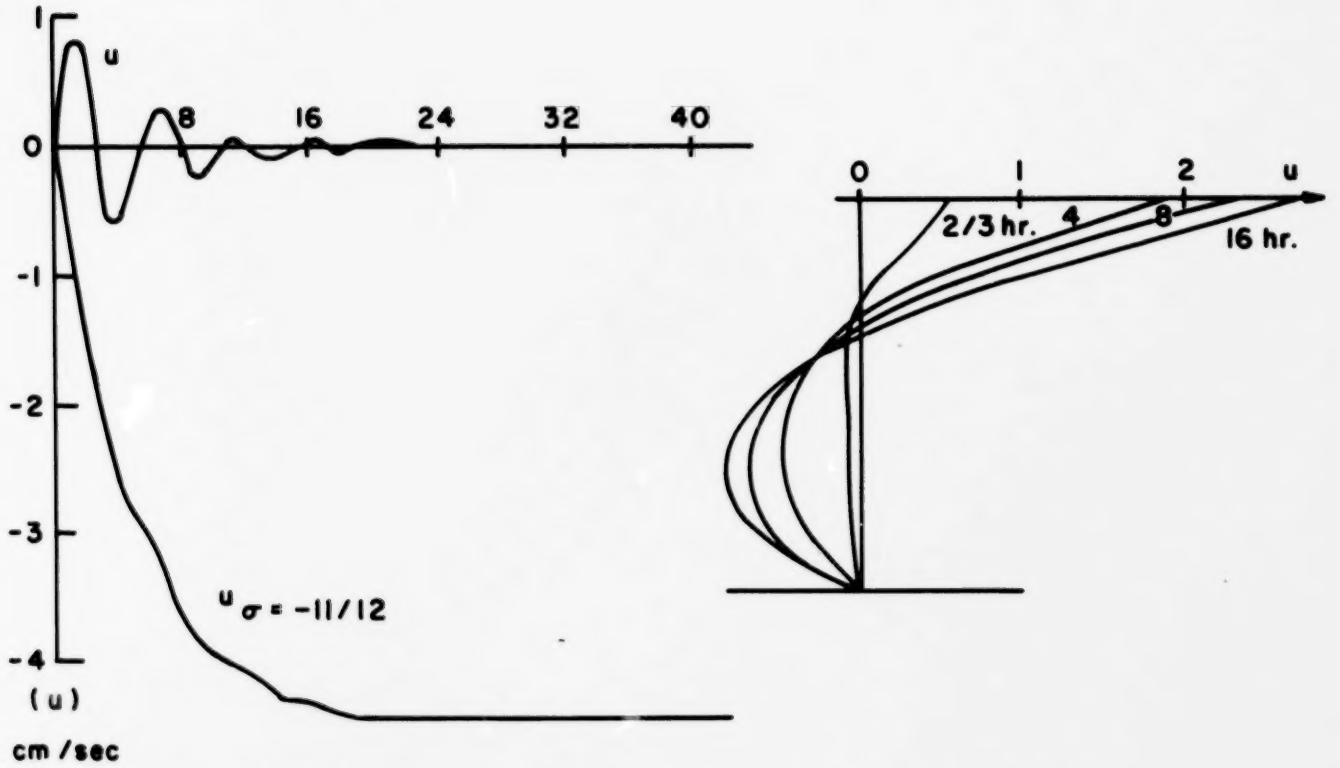

Figure 5.3. (a) Integrated current and near-bottom current, and
(b) Vertical profile of horizontal currents at point 2 of Fig. 5.1.

The surface elevations at two locations in the basin, shown in Figure 5.4, clearly indicate a period of oscillation of 2.5 hours corresponding to the seiche oscillation in the basin. As can be seen, the surface elevations compare well with those computed by a single-mode free-surface model with $\Delta t = 5$ min.

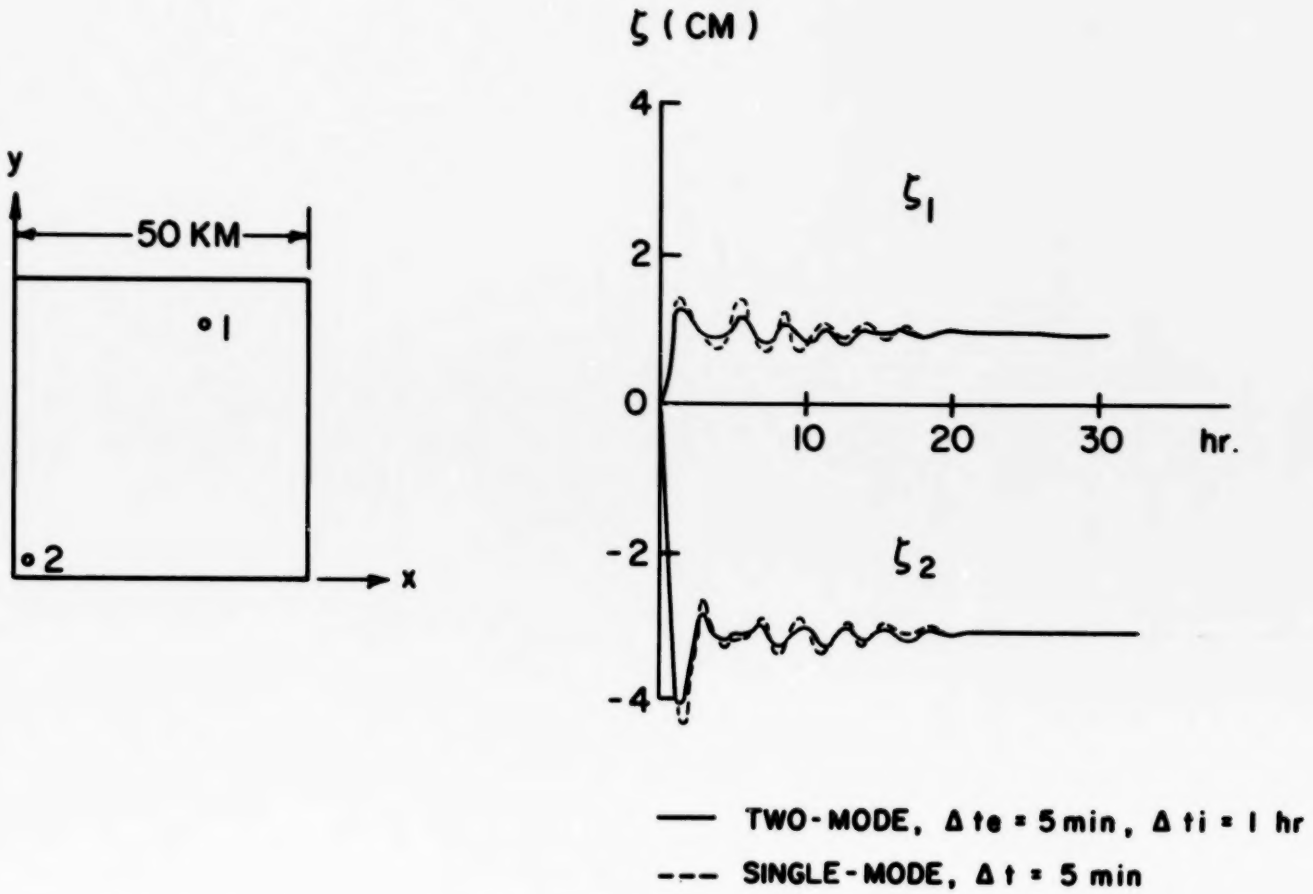

Figure 5.4 Results in a constant-depth square basin.

SECTION 6

APPLICATIONS TO LAKE ERIE

Lake Erie (Figure 6.1) is composed of three basins, a shallow Western Basin, a larger and relatively flat, but deeper Central Basin, and a cone-shaped and deep Eastern Basin. The average depths of the Western, Central, and Eastern Basin are 7, 18, and 24 meters respectively.

The three-dimensional free-surface model as described in previous sections has been applied to Lake Erie. The results are being used to compute the transport and resuspension of sediments in the Western Basin of Lake Erie. The output is being compared with data from coordinated aircraft/ship surveys by the National Aeronautics and Space Administration. (Sheng and Lick, 1977a; 1977b.)

For sufficient accuracy, a 1.6 km horizontal numerical grid is used in the Western Basin and a portion of the Central Basin and is coupled with a 12.8 km grid in the rest of Lake Erie (Figure 6.2). Five grid points in the vertical direction are used. The flows in the fine and coarse grids are coupled dynamically and calculated simultaneously in time to allow full interaction between the two grids (Sheng, 1975; Sheng and Lick, 1976). The coupling scheme has been shown to produce smooth results across the fine and coarse grids without appreciable computational reflections. In the present analysis, three islands in the Western Basin are included as are river flows from the Detroit River, the Maumee River, and the Sandusky River and outflow to the Niagara River.

As a boundary condition, the wind stress at the lake surface needs to be specified. For the relation between the wind stress and wind velocity, it is assumed that

$$\underline{\tau}^{w} = \rho_a C_D W_a \underline{W}_a \tag{6.1}$$

where $\underline{\tau}^{w}$ is the wind stress vector, ρ_a is the air density, C_D is a skin-friction coefficient, W_a is the magnitude of the wind velocity while $\underline{W}_a$ is the wind velocity vector. The coefficient C_D is taken to be 0.00273 for strong winds (W_a exceeds 6 m/sec) and 0.00166 for light winds, where $\underline{W}_a$ is measured at 6 m above the lake surface (Wilson, 1960).

To obtain the wind stress over the entire lake under variable wind conditions, an interpolation scheme has to be applied to the irregularly spaced date recorded at weather stations around the lake. Interpolation with weighted averages based on an inverse square of the distance from weather stations has been used (Platzman, 1963):

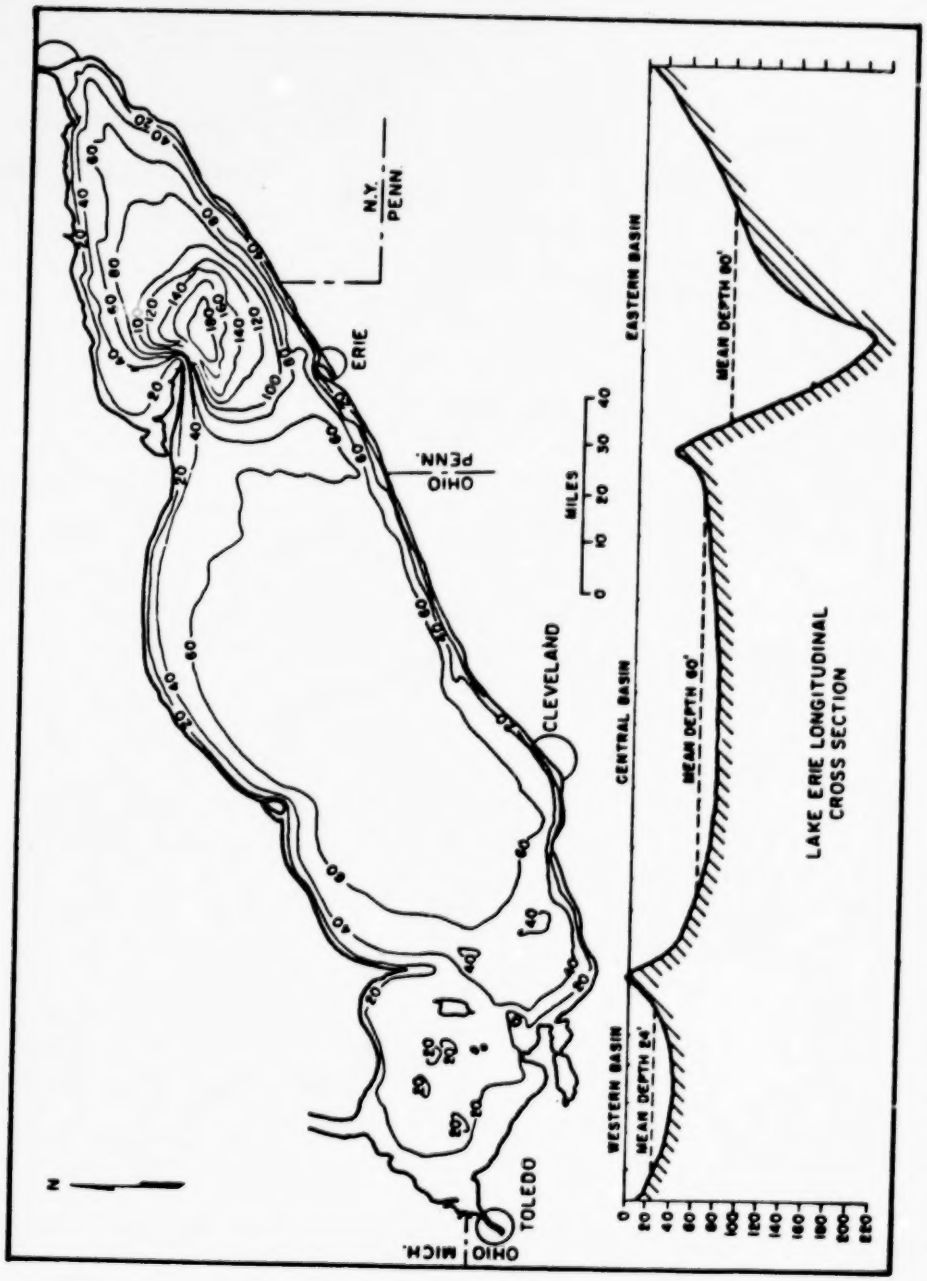

Figure 6.1 Lake Erie bottom topography.

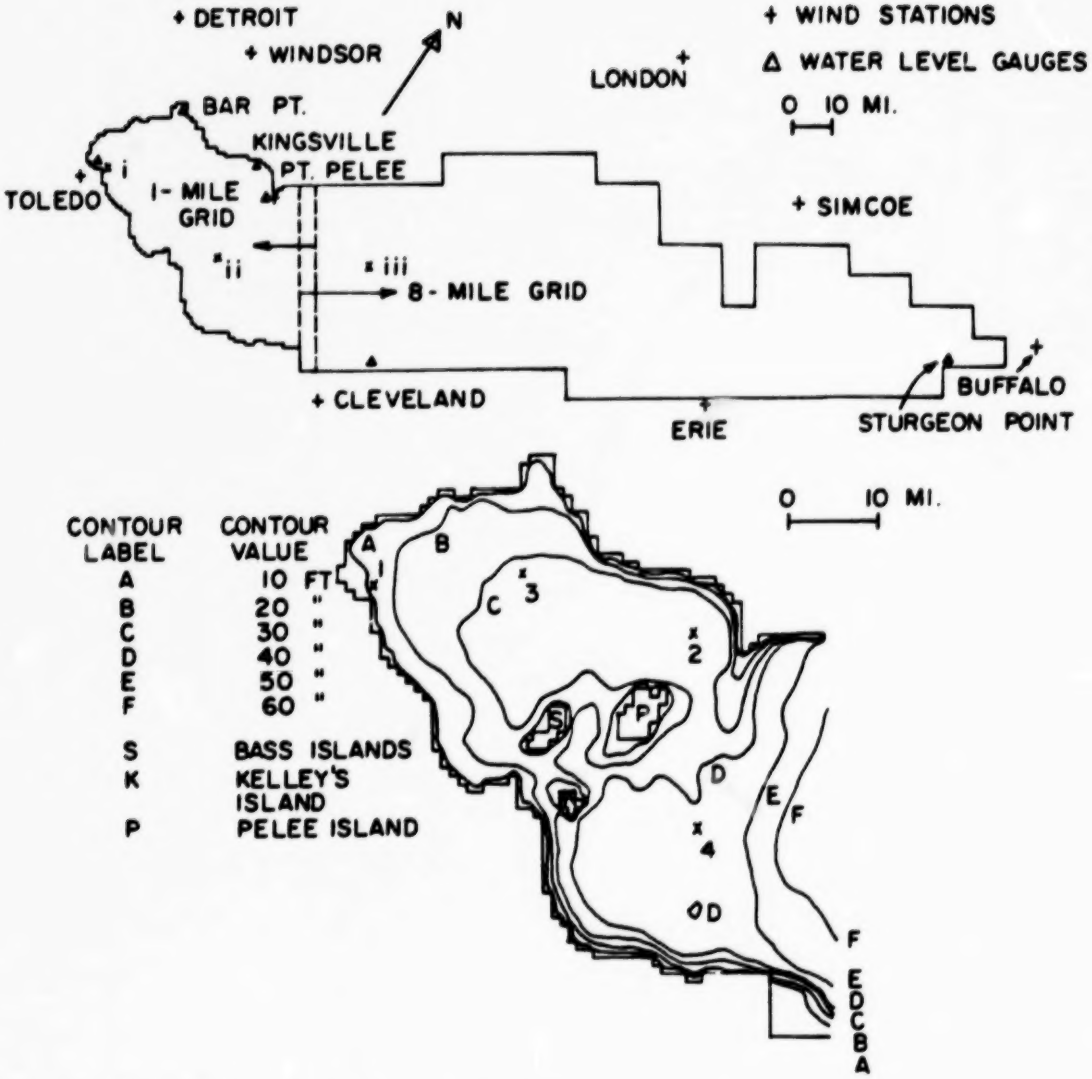

Figure 6.2 (a) Numerical grid structure of Lake Erie and locations of wind stations and water level gauges.
(b) Bottom topography of Western Lake Erie.

$$\underline{\tau}^{w}(x,y,t) = \sum_{m} \lambda_{m}(x,y)\, \underline{\tau}_{m}^{w}(t) \qquad (6.2)$$

where $\underline{\tau}_{m}^{w}$ is the wind stress as derived from the wind velocity at station m, where λ_m is a dimensionless weighting function given by

$$\lambda_{m}(x,y) = \frac{r_{m}^{-2}}{\sum_{A} r_{n}^{-2}} \qquad (6.3)$$

and where $r_m = [(x-x_m)^2 + (y-y_m)^2]^{0.5}$ is the distance between the point (x,y) and the station (x_m,y_m). To account for the difference between winds over the water and over the land, the stress actually used in the calculations was the stress from Eq. (6.2) multiplied by 1.5. In the interpolation, data from nine weather stations (Figure 6.2) were used.

In the numerical computations, the external mode of the free-surface model is limited by a time step $\Delta t_e \leq x/(2gh)^{0.5} = 81$ sec, while the internal mode is limited by $\Delta t_i \leq h_{min}^2/2A_v = 1500$ sec (based on $h_{min} = 2.7m = 9$ ft). The external time step was taken to be 75 sec and the internal step to be 900 sec. A vertical eddy coefficient A_v of 25 cm^2/sec was assumed. When the horizontal turbulence terms were included in the equations, a horizontal eddy coefficient A_H of $10^6 cm^2$/sec was assumed.

Constant Wind

As a first example, the time-dependent currents caused by a suddenly imposed constant wind of 5.2m/sec from W67S were calculated. It was assumed that the lake was calm initially. Calculations were carried out for 24 hours. Although a suddenly imposed, constant wind is an idealized situation, it serves as a simple example. Some weather systems may be approximated by such a wind.

The computed results indicate that initially mass is transported in the direction of the wind from the western end of the lake to the eastern end. About seven hours after the start of the wind, the mass flow in the interior of the lake begins to reverse its direction while the mass flow in the shallow coastal regions is still in the direction of the wind. The surface elevation versus time at three locations in the western portion of the lake is shown in Figure 6.3. Periods of seiche oscillation in the longitudinal direction (14 hours) and in the transverse direction (2 to 3 hours) are apparent. The surface elevation approaches a steady state in about 24 hours. In the Central and Eastern Basins, however, the steady state is approached in about two to four days. The horizontal velocities at three hours after the initiation of the flow are shown in Figure 6.4 for every 3.2 km interval in the x and y directions. Figure 6.4 shows the horizontal velocities near the surface ($\sigma = 0.1$). It can be seen that the near-surface currents are from the Western into the Central Basin and are deflected somewhat to the right of the wind. A similar flow pattern is also apparent at mid-depth ($\sigma = 0.5$) as shown in Figure 6.4b. It can be shown that the computed results continue to show currents from the Western to the Central Basins at all depths until about 7 hours at which time strong opposing cur-

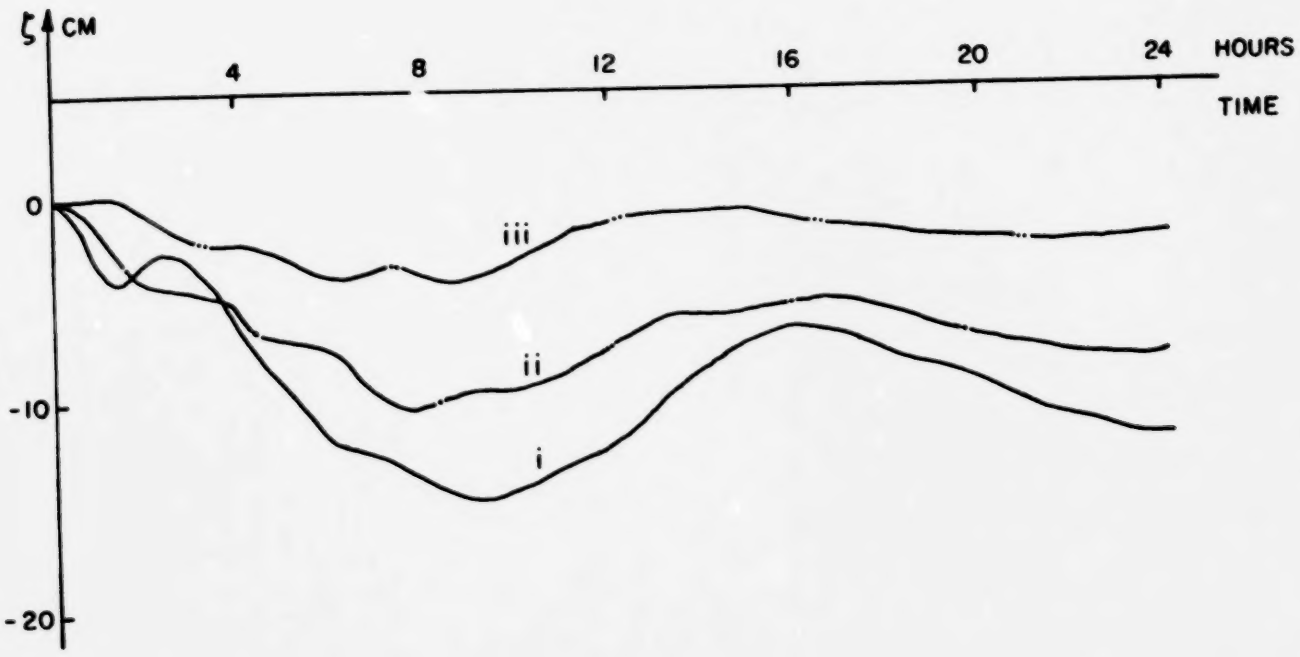

Figure 6.3 Surface elevation computed by free-surface model as a function of time at three locations in Lake Erie. The wind is constant with a velocity of 5.2 m/sec from W 67 S.

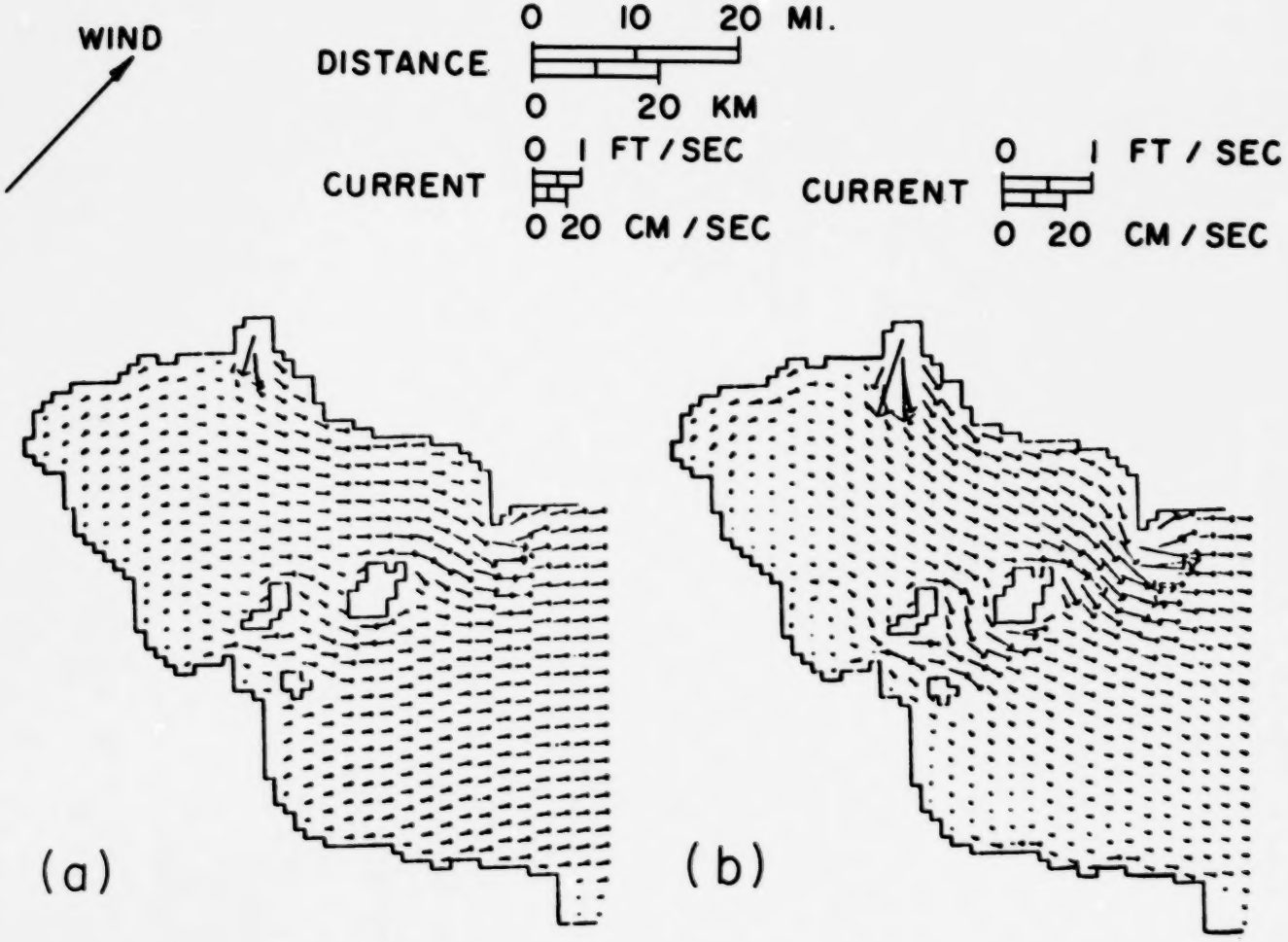

Figure 6.4 Horizontal velocities at a constant (a) 0.1 depth and (b) 0.5 depth from surface after 3 hours. The wind is constant with a velocity of 5.2 m/sec from W 67 S .

rents develop. The currents continue to oscillate with time until about 24 hours when a steady state is approximately reached. The steady-state currents as shown in Figure 6.5 compare well with the results of a steady-state model (Gedney and Lick, 1971).

Variable Wind

The time-dependent flow in Lake Erie caused by actual wind conditions during a two-day period from March 7 through March 8, 1976 was also calculated. For this period, Figure 6.6 shows the wind speed as a function of time at several weather stations around the lake. It can be seen that the winds were generally quite strong on March 7, on the order of 20 knots, and gradually decayed on March 8 to below 10 knots. To generate the required stress field for the numerical computation, hourly wind data over the regular numerical grid were obtained by interpolation of the irregularly spaced wind data at 9 weather stations (Figure 6.2). The lake was assumed to be calm initially at 00:00 on March 7. Calculations were made for 48 hours until 00:00 March 9.

As a verification of the model, the computed surface elevations were compared with water level data recorded by several gauges on Lake Erie operated by the U.S. Ocean Survey. The results for the surface elevations at Toledo, Bar Point, Point Pelee, Cleveland, and Sturgeon Point are shown in Figure 6.7. The observed curves were obtained by subtracting the 24-hour running mean of the sum of all stations from the recorded lake level data. The longitudinal seiche period of 14 hours, on which is superimposed the transverse seiche period of 2 to 3 hours, is again apparent. Reasonable agreement between computed and observed data exists at all stations except during the initial 12 hours.

The largest discrepancy between computed and observed data occurs at Bar Point. This is probably due to the incorrect specification in the analysis of the Detroit River which would clearly affect the water level in the vicinity of the river. Although the flow rate at the mouth of the Detroit River is generally time-varying and should depend on wind conditions, detailed measurements of the flow rate during the time period of this study were not available and the flow was assumed to be constant.

Figure 6.8 shows the horizontal velocities versus time near the surface ($\sigma = 0.1$) and at mid-depth ($\sigma = 0.5$) at two locations in the Western Basin (indicated at points 1 and 2 in Figure 6.2). The longitudinal and transverse seiches are clearly identifiable at both locations. The transverse seiche is more pronounced at point 1.

By comparing the time histories of the velocities at points 1 and 2 with the time histories of the wind stresses and surface elevations at nearby stations, it is apparent that the currents at point 1 correlate more closely with the wind stresses whereas the currents at point 2 correlate more closely with the surface elevations. This can be understood as follows. At point 1 near Toledo where the depth is shallow and the winds are strong, the currents at all depths are primarily driven by the wind, and the influence of the pressure gradient caused by tilting of the free surface is

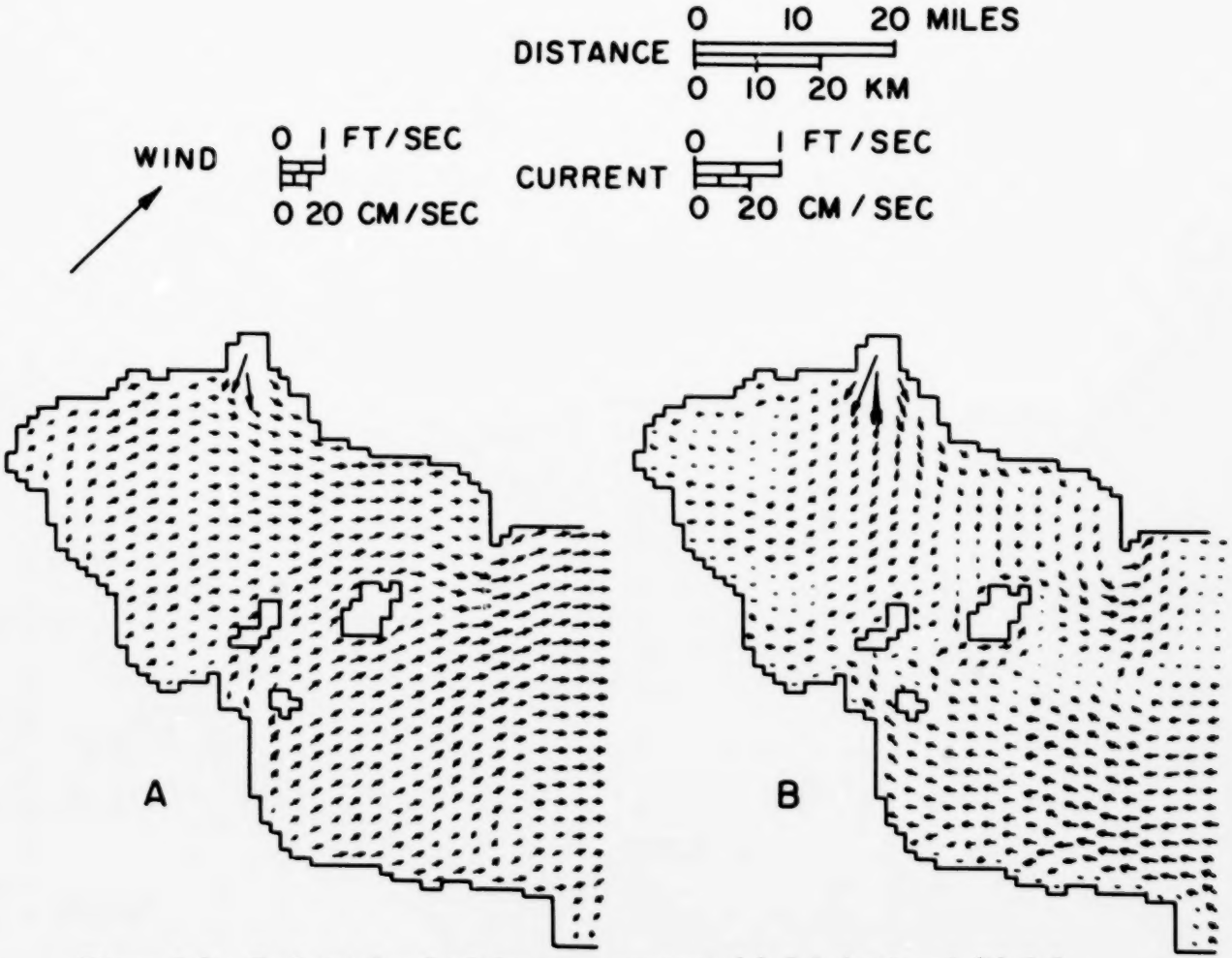

Figure 6.5. Horizontal velocities at a constant (a) 0.1 depth and (b) 0.5 depth from surface after 24 hours. The wind is constant with a velocity of 5.2 m/sec from W 67 S.

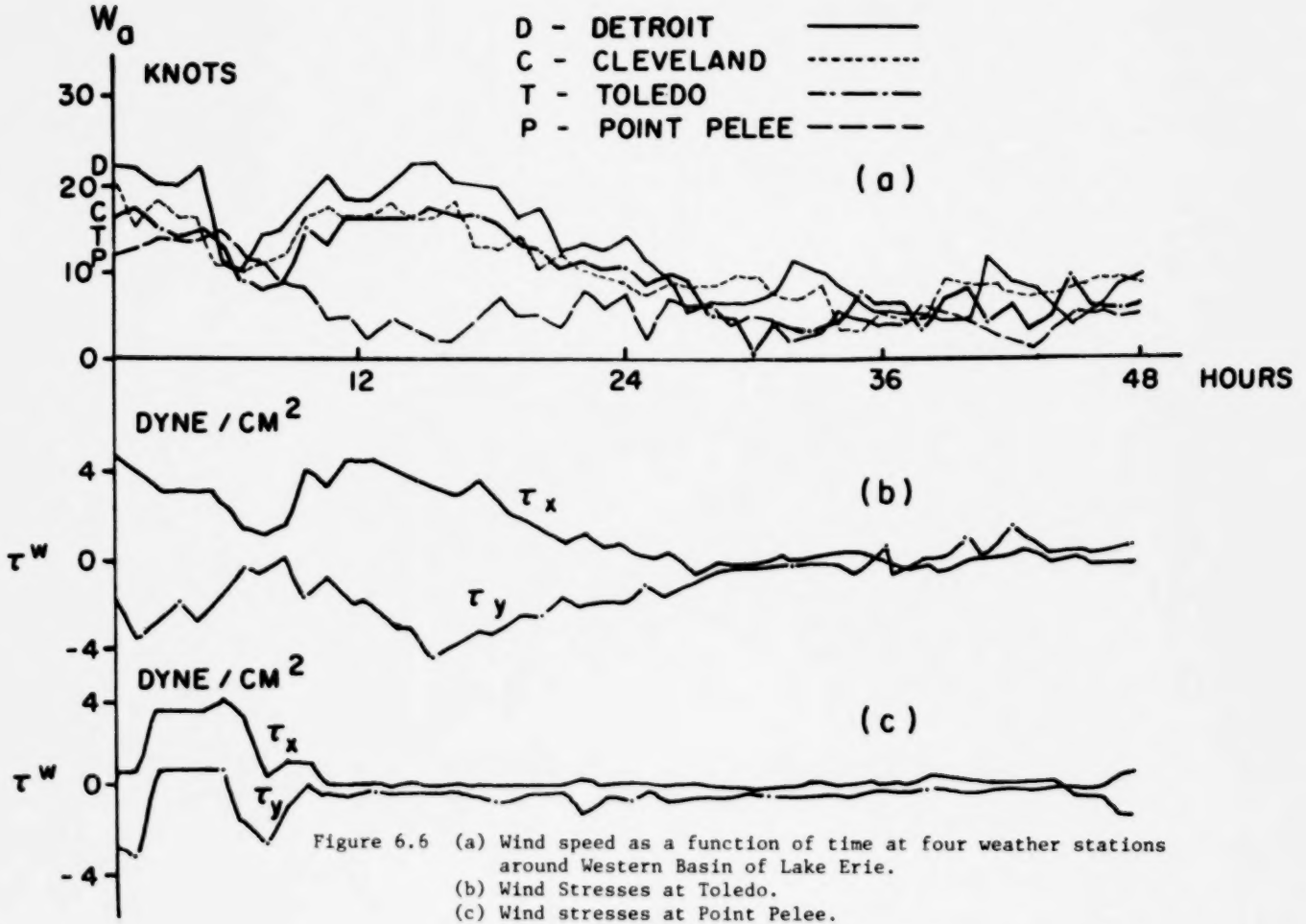

Figure 6.6 (a) Wind speed as a function of time at four weather stations around Western Basin of Lake Erie.
(b) Wind Stresses at Toledo.
(c) Wind stresses at Point Pelee.

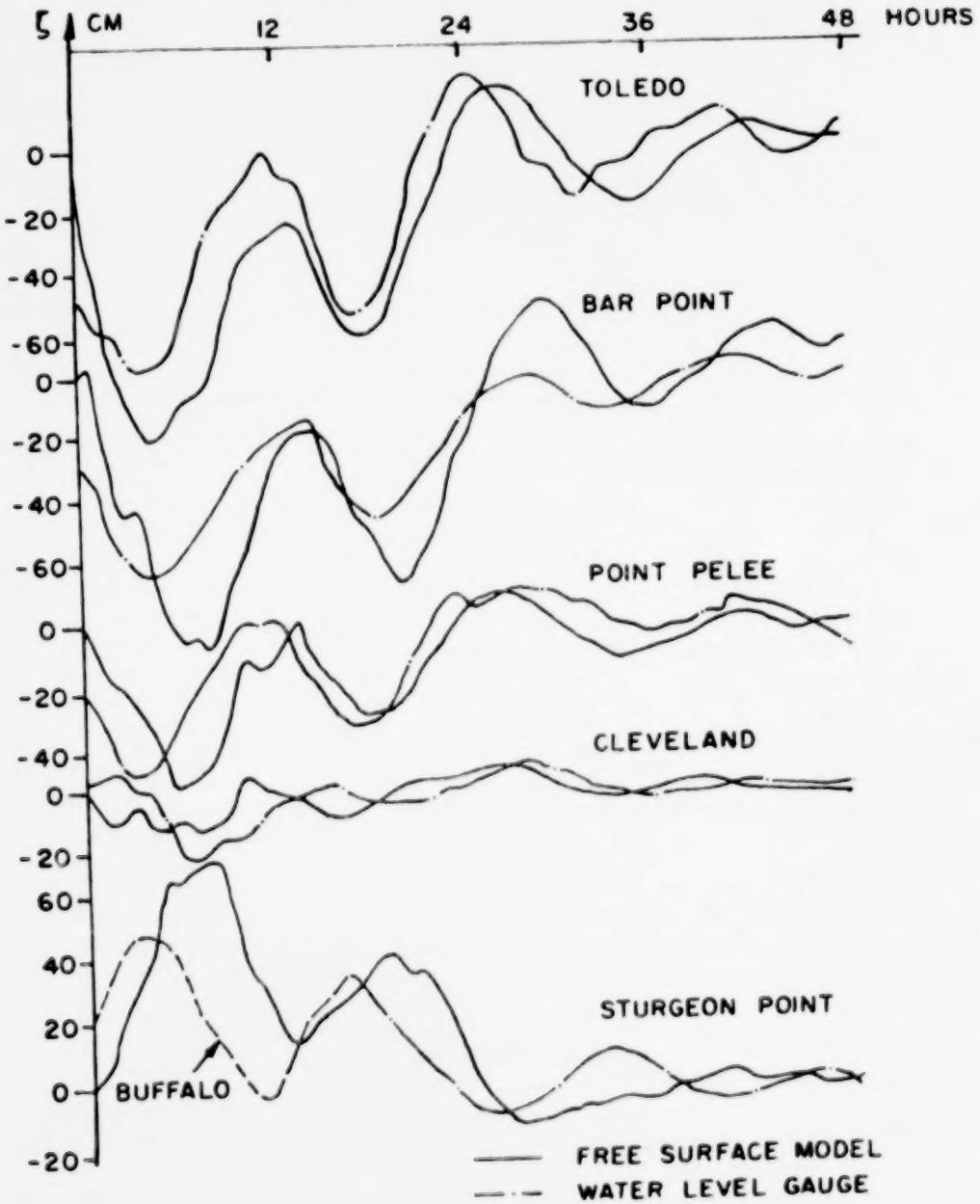

Figure 6.7 Comparison of surface elevation computed by free surface model with water level measurement at 5 gauges.

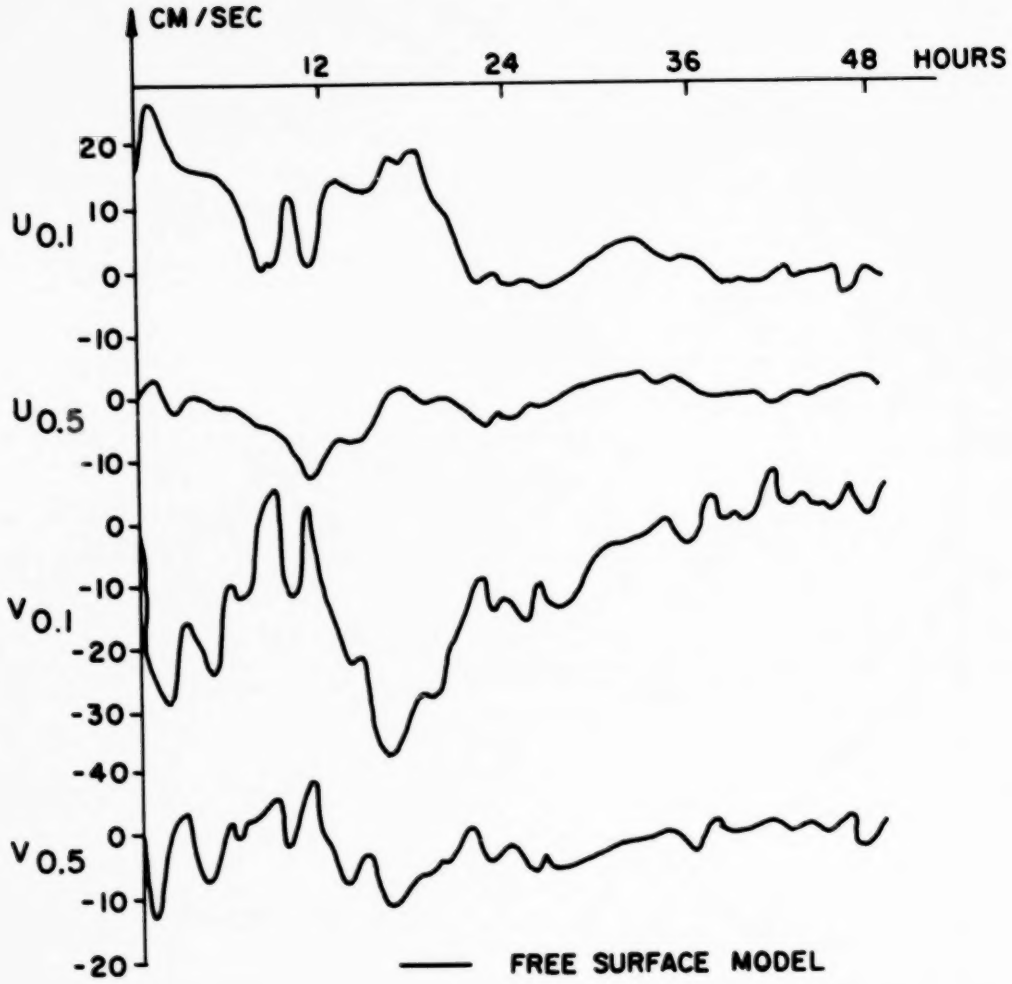

Figure 6.8a. Horizontal velocities at 0.1 depth and 0.5 depth as function of time at station 1 (near Toledo).

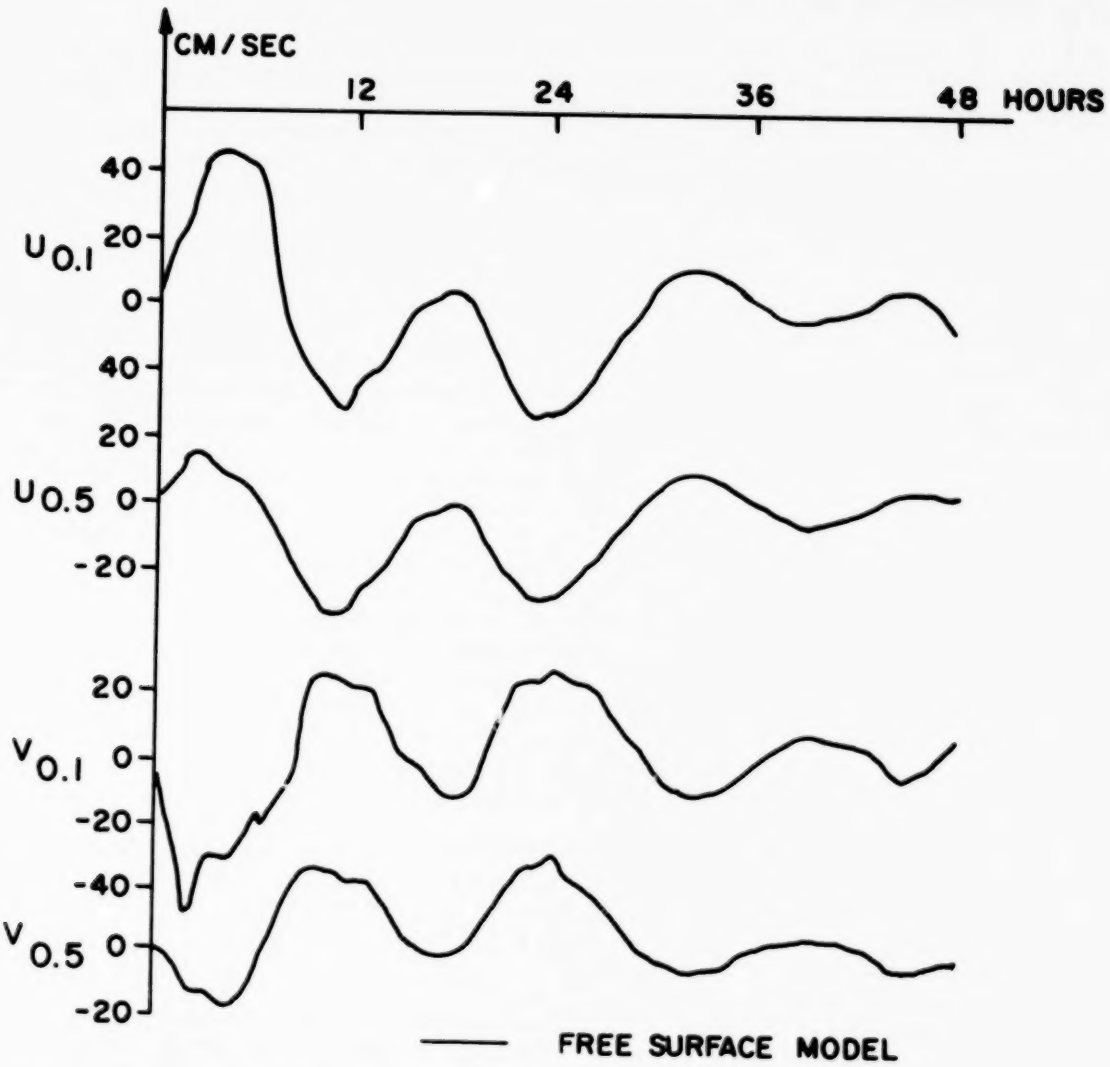

Figure 6.8b. Horizontal velocities at 0.1 depth and 0.5 depth as function of time at station 2 (near Point Pelee).

relatively small. However, at point 2 near Pt. Pelee where the depth is greater and the winds are weaker during the two-day period, the currents at all depths are more influenced by the pressure gradient which in turn is significantly affected by surface oscillations due to gravity waves.

The horizontal distribution of currents at several times are shown in Figures 6.9 to 6.12. During the first 24 hours, due to the strong winds and the start-up of the flow, the instantaneous currents are generally quite strong. The currents (at σ = -0.1 and -0.5) at 0600 3/7/76 and 1200 3/7/76 are shown in Figures 6.9 and 6.10 respectively. It is interesting to note that the currents between the islands and in the Pelee Passage are generally quite strong compared to the currents in other regions. The near-surface currents and the mid-depth currents are primarily in the same direction.

At 0000 3/8/76, although the winds are predominantly from the Northwest, the results show strong opposing currents at all depths (Figure 6.11) due to the mass flux from the Central Basin into the Western Basin associated with the free-surface movement. Maximum currents near the surface and at mid-depth are on the order of 100 cm/sec and 60 cm/sec, respectively.

At 1200 3/8/76, the winds have decreased further and are relatively mild. As shown in Figure 6.12, the currents are still quite significant. It is of particular interest to note the presence of a large eddy off Point Pelee. From the calculation, it can be shown that this large eddy existed throughout the water column for approximately 1.5 hours. The presence of such an eddy off Point Pelee of similar scale has been observed by the LANDSAT satellites quite frequently. Figure 6.13 shows the eddy observed on April 14, 1973. Unfortunately, LANDSAT satellites were not over Lake Erie on 3/8/76. The horizontal currents computed by a rigid-lid model indicate very weak currents at 1200 3/8/76 (Figure 6.14). The fact that the large eddy is not present in the rigid-lid results indicates that seiche oscillation is an important cause of the observed eddy.

At 0000 3/9/76, the winds have decreased further and the flow in the northern portion of the Western Basin showed opposing currents at mid-depth and near the surface, indicating a quasi steady-state (Figure 6.15).

Comparison With A Rigid-Lid Model

The above calculations of the time-dependent flow in Lake Erie were repeated using the rigid-lid model of Paul and Lick (1974, 1979). The results of the present two-mode free-surface model and the rigid-lid model were compared by Sheng et al. (1978). For relatively short time intervals, significant differences between the results of the two models occur as expected since the seiche motion is eliminated in the rigid-lid model. The horizontal velocities at point 1 near Toledo and point 2 near Pt. Pelee as computed by the two models are shown in Figures 6.16 and 6.17. Based on comparisons made at four locations in the Western Basin, the two results differ most at point 2, the pressure-driven station, and differ least at point 1, the wind-driven station.

The rigid-lid results tend to represent a filtered version (i.e., a

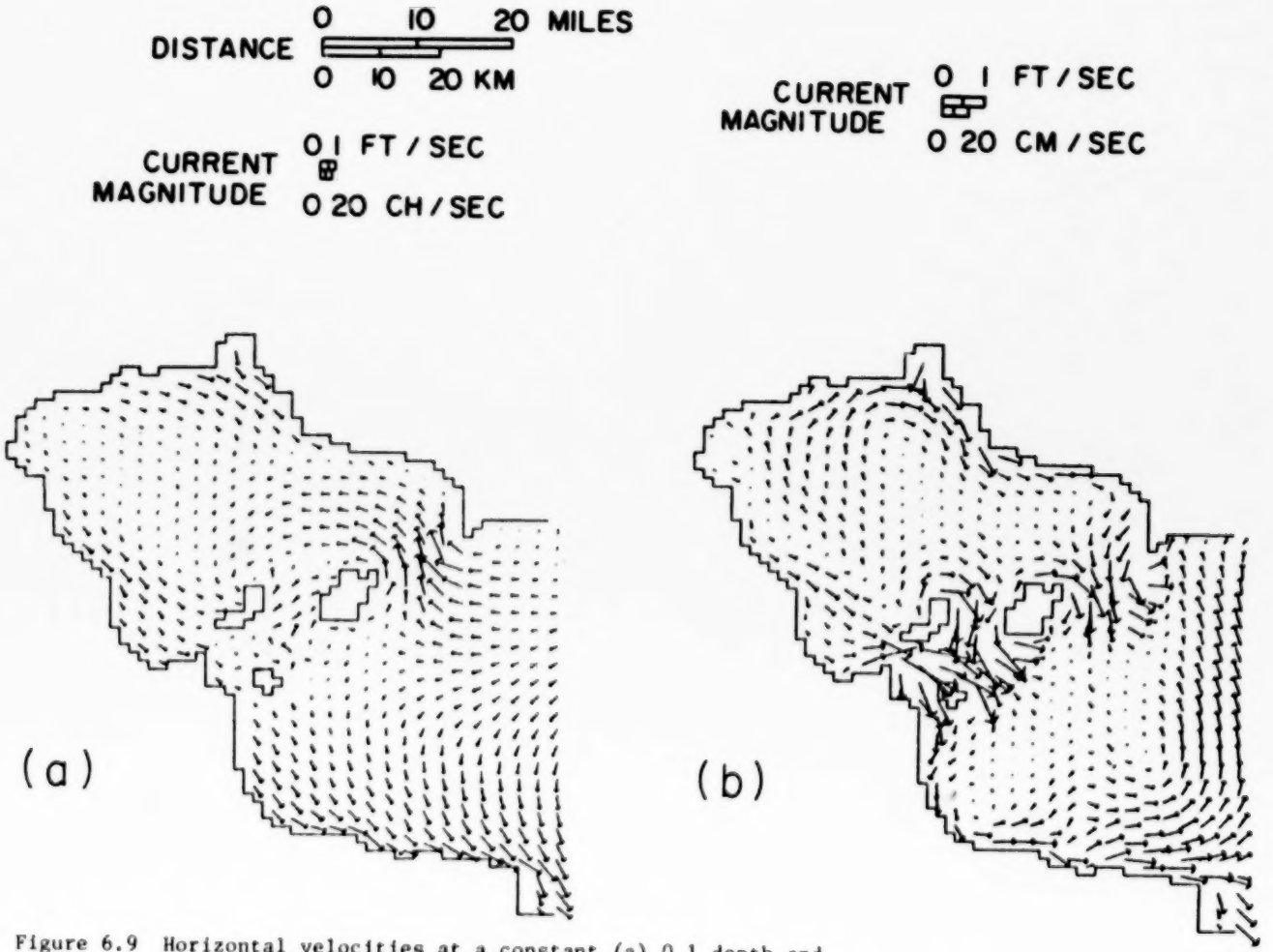

Figure 6.9 Horizontal velocities at a constant (a) 0.1 depth and (b) 0.5 depth from the surface at 0600 3/7/76.

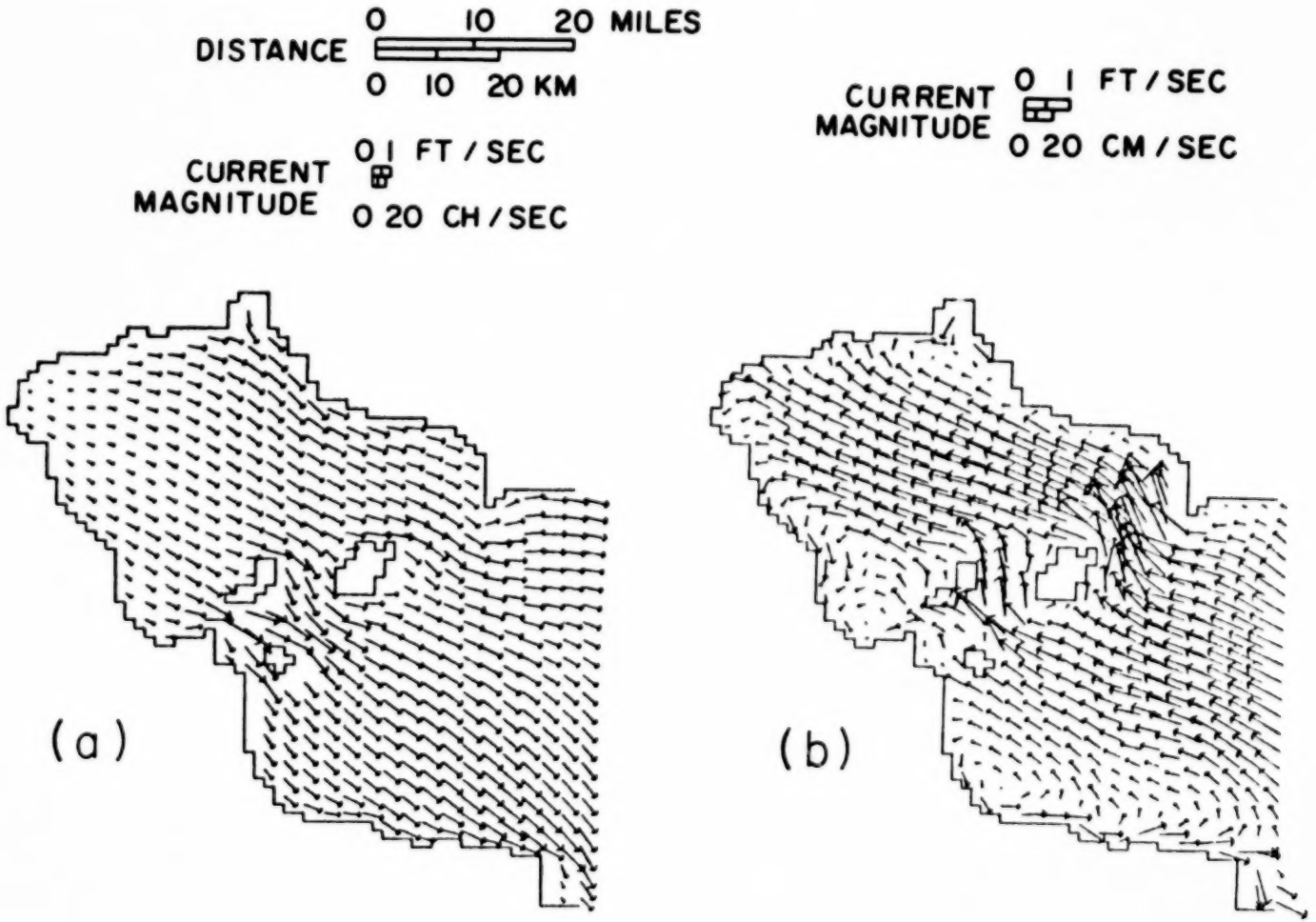

Figure 6.10 Horizontal velocities at a constant (a) 0.1 depth and (b) 0.5 depth from the surface at 1200 3/7/76.

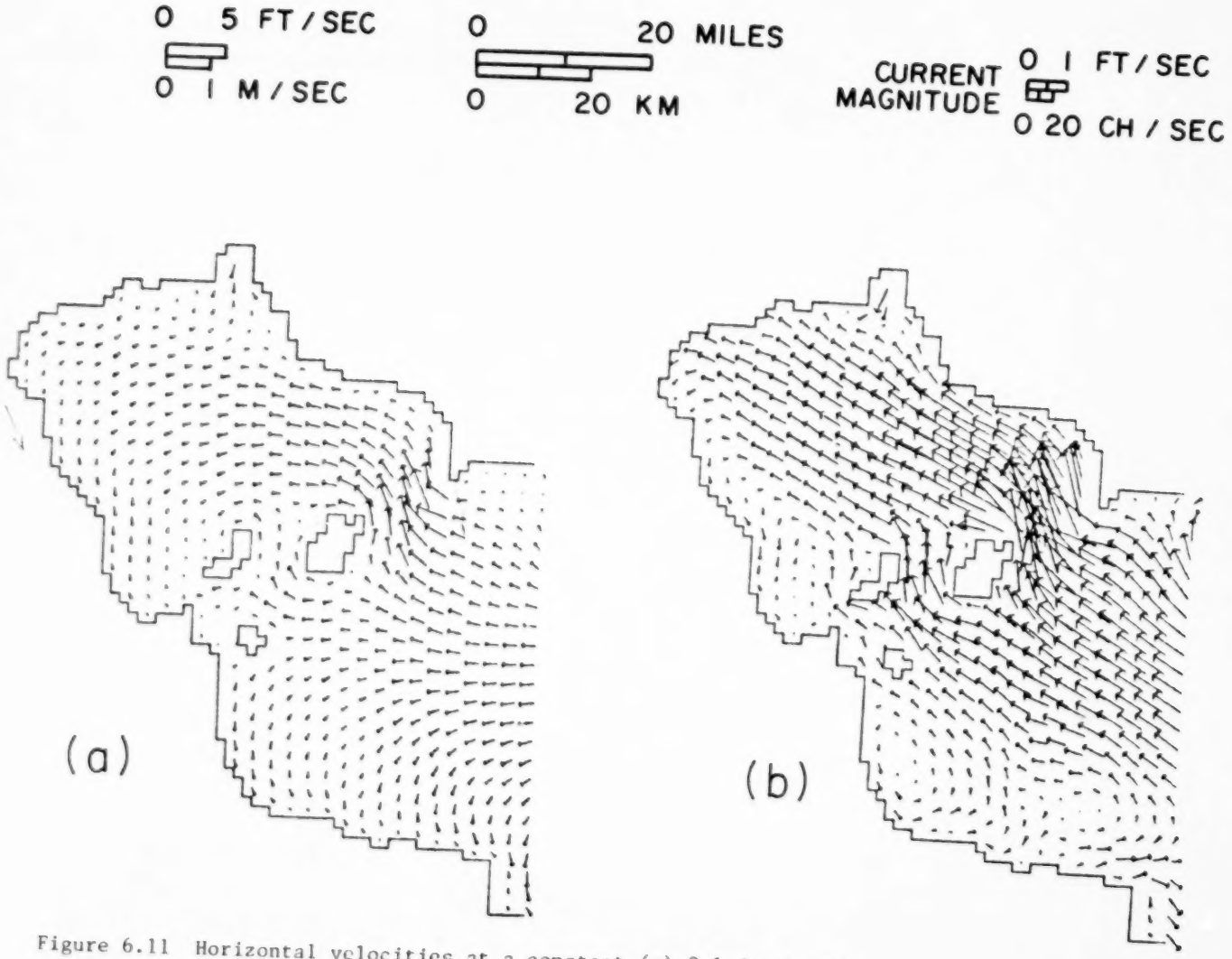

Figure 6.11 Horizontal velocities at a constant (a) 0.1 depth and (b) 0.5 depth from the surface at 0000 3/8/76.

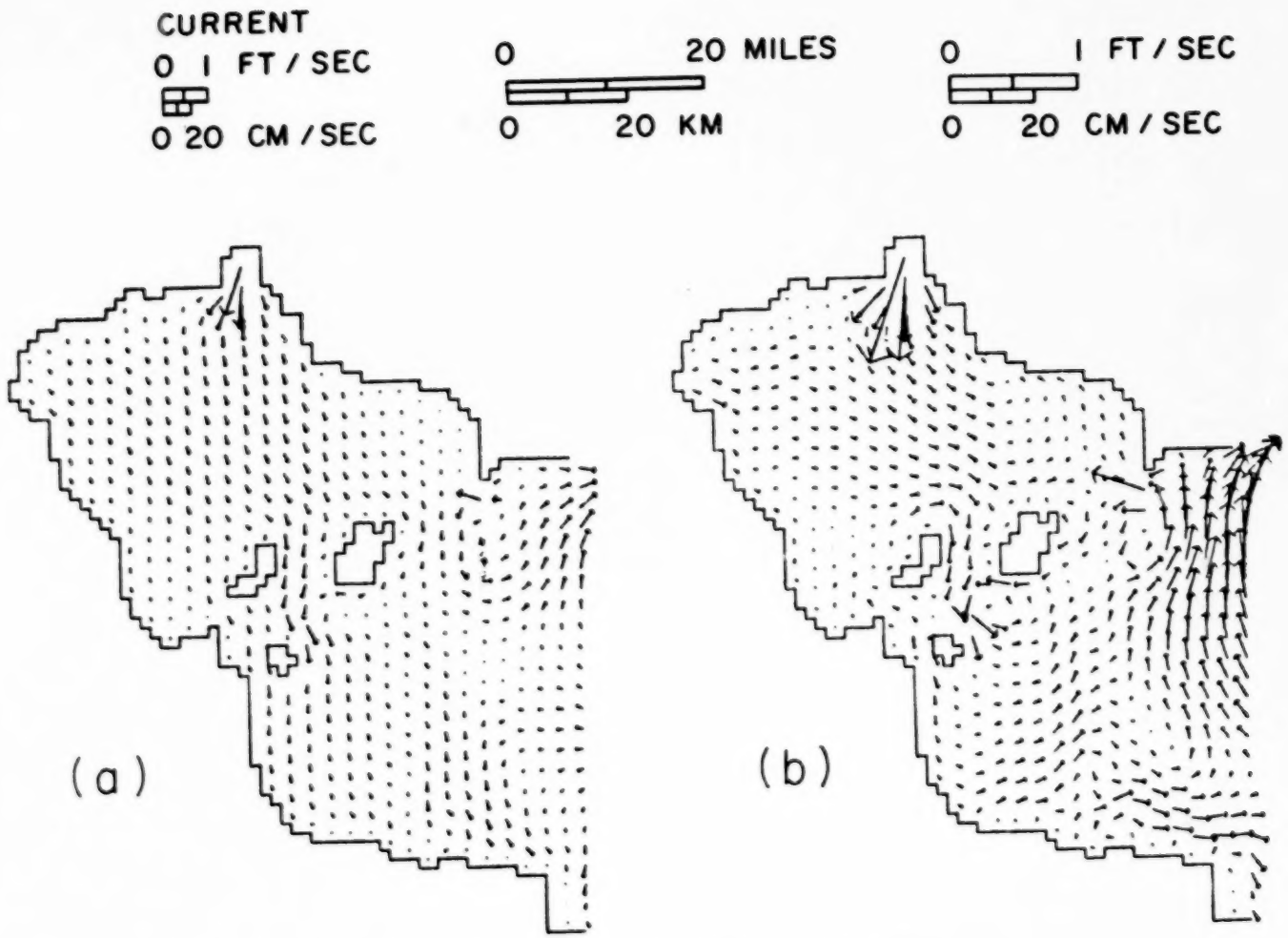

Figure 6.12 Horizontal velocities at a constant (a) 0.1 depth and (b) 0.5 depth from the surface at 1200 3/8/76.

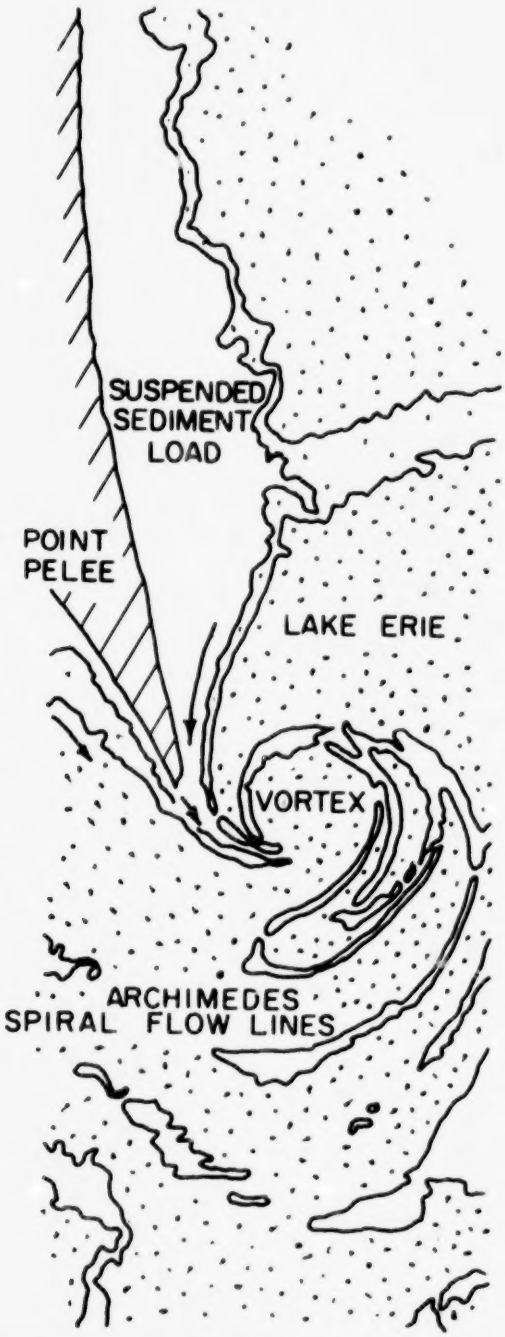

Figure 6.13. Large-scale eddy observed by ERTS-1 (LANDSAT-1) off the tip of Point Pelee on 3/14/73.

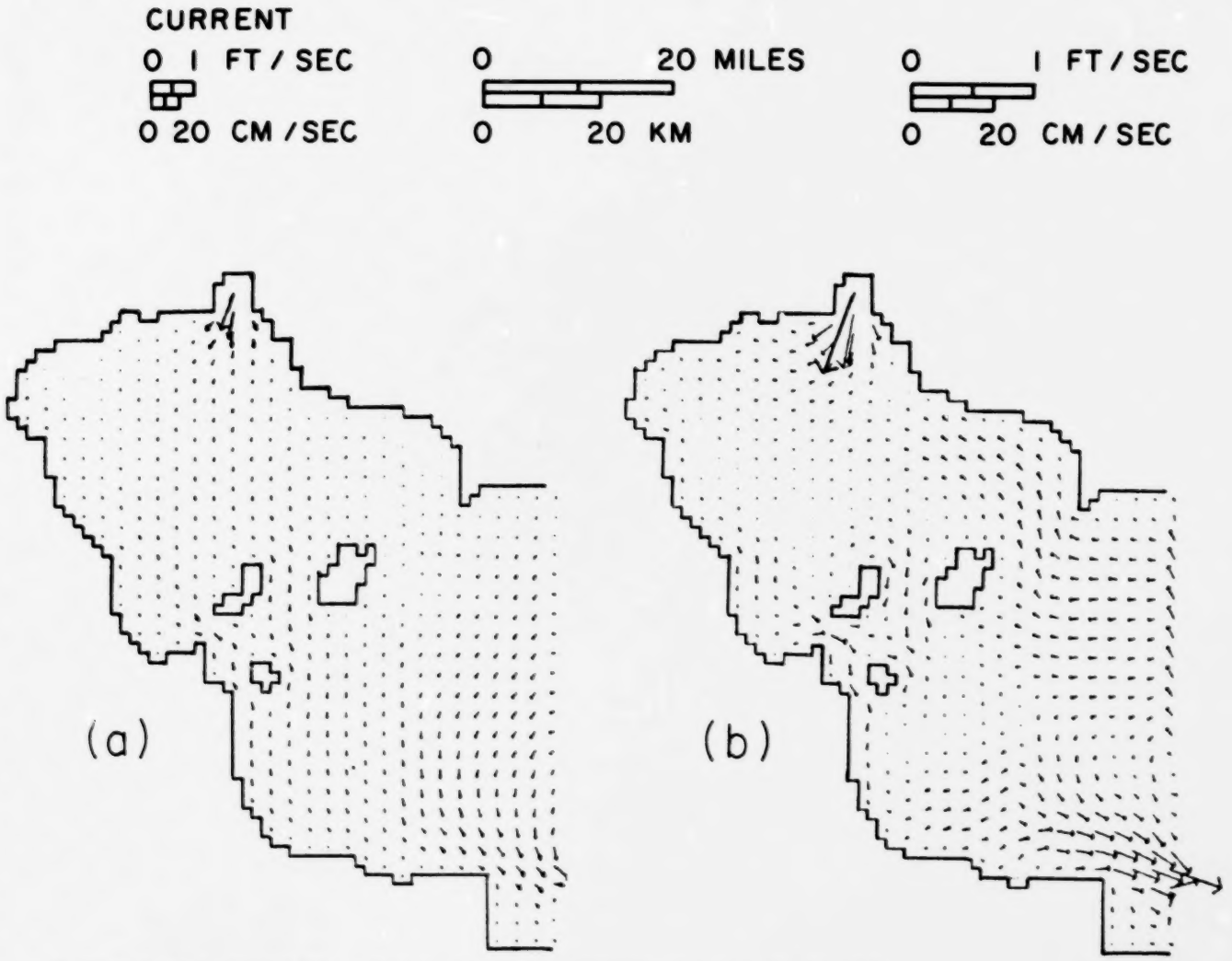

Figure 6.14 Horizontal velocities at a constant (a) 0.1 depth and (b) 0.5 depth from the surface at 1200 3/8/76.

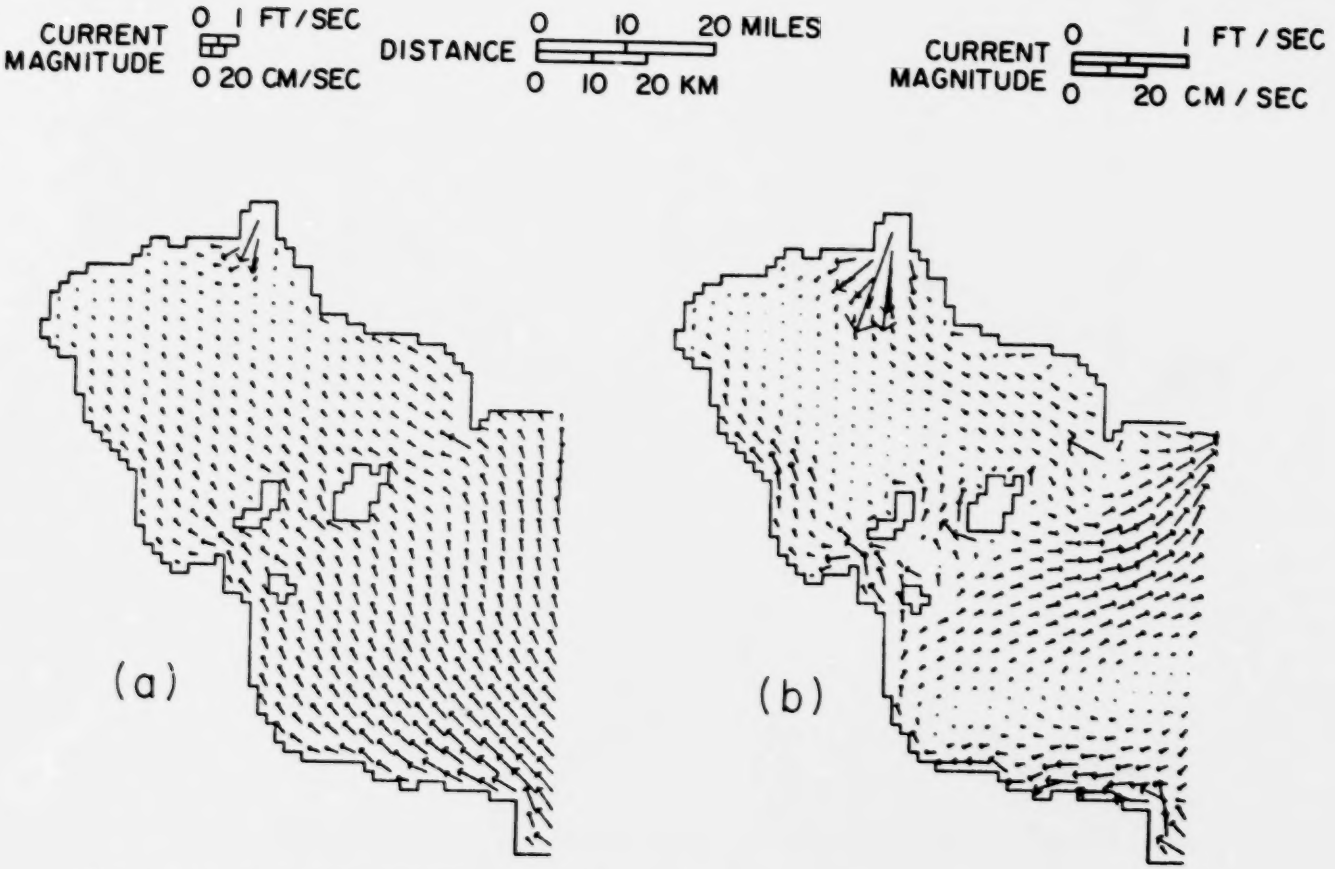

Figure 6.15 Horizontal velocities at a constant (a) 0.1 depth and (b) 0.5 depth from the surface at 0000 3/9/76.

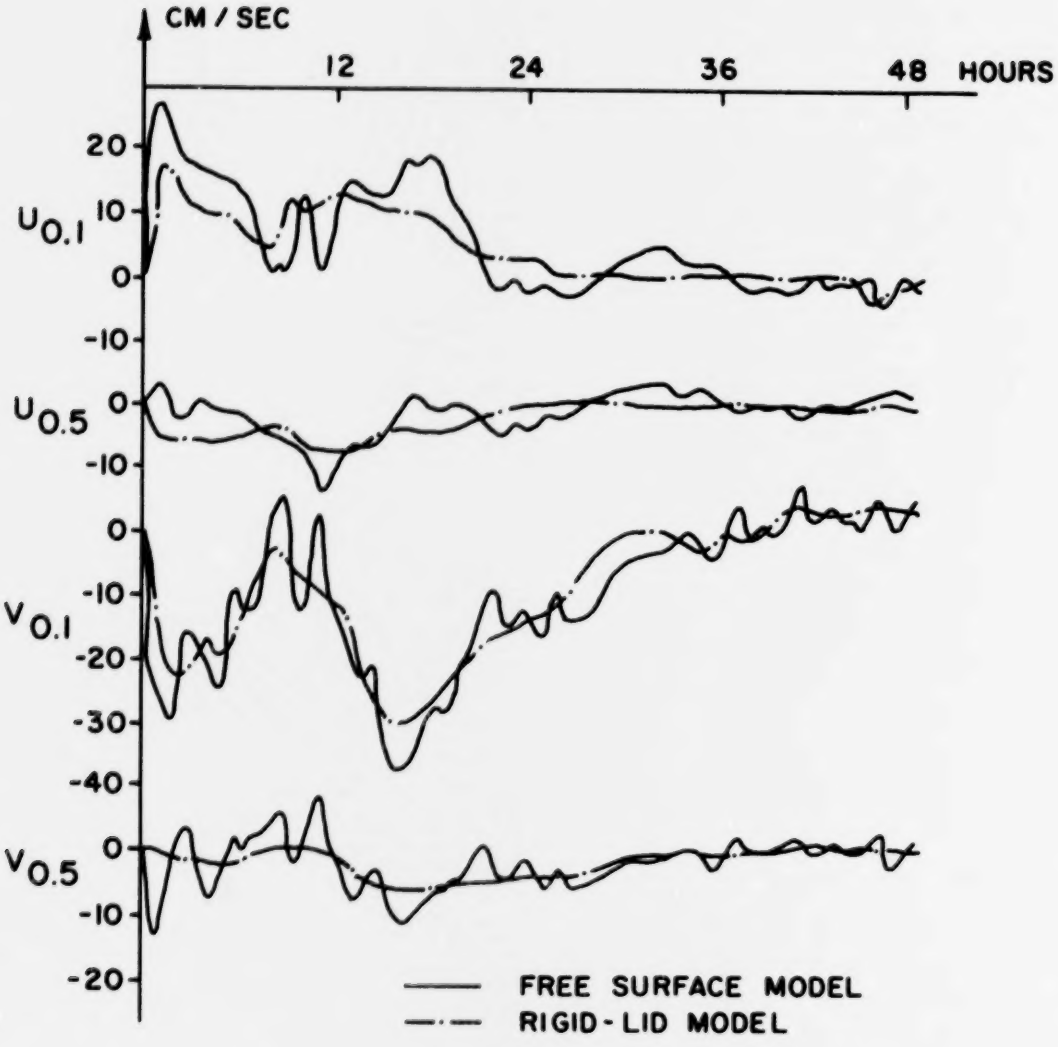

Figure 6.16. Horizontal velocities at 0.1 depth and 0.5 depth as function of time at station 1 (near Toledo).

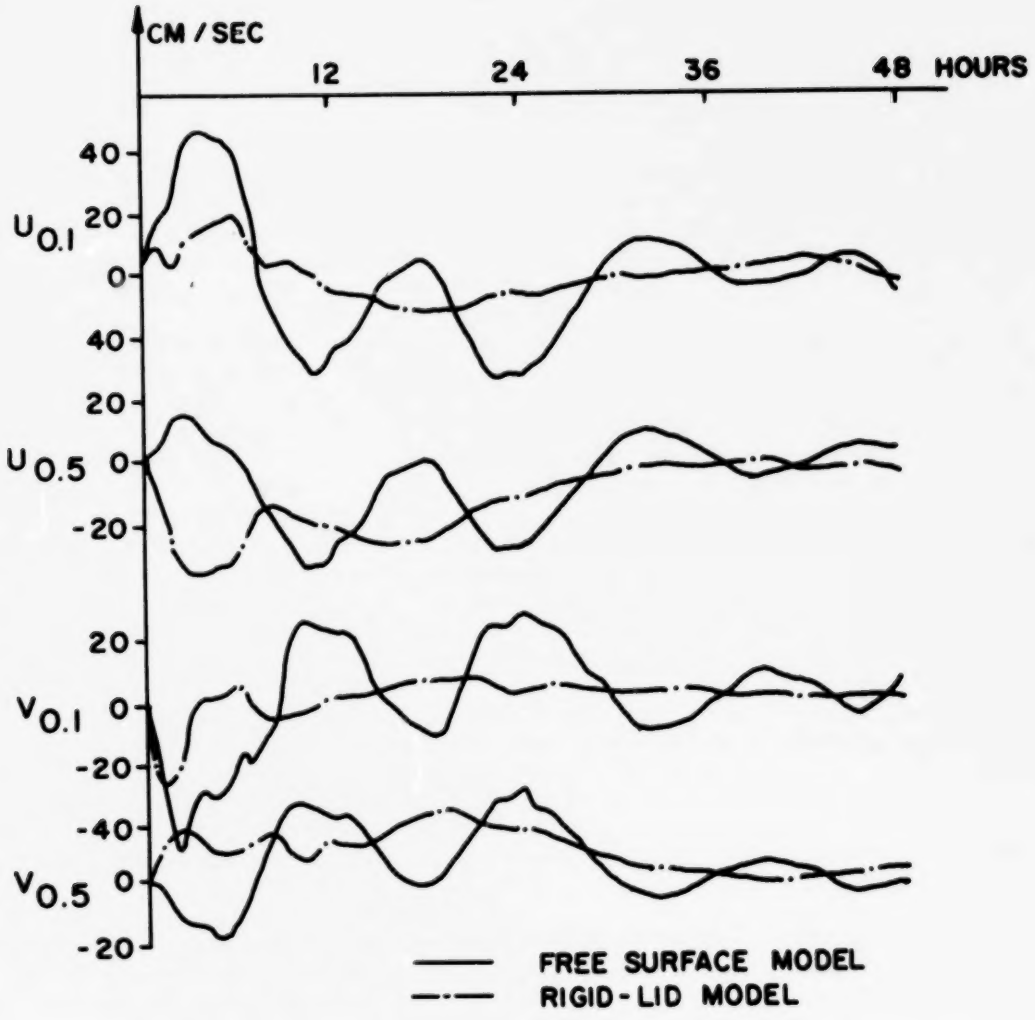

Figure 6.17. Horizontal velocities at 0.1 depth and 0.5 depth as function of time at station 2 (near Point Pelee).

version in which the seiche oscillations are eliminated) of the free-surface results. Hence it is of interest to compare the two models in terms of time-averaged currents over periods of one or more dominant seiche cycles. The instantaneous currents at points 1 and 2 have been averaged over three 14-hour periods (0-14, 14-28, 28-42) and also over the entire 42-hour period and are shown in Figures 6.18 and 6.19. As can be seen in Figure 6.18, the time-averaged currents at point 1 as computed by the two models agree well except during the third seiche cycle. However, as shown in Figure 6.19, the time-averaged free-surface and rigid-lid currents at point 2 are significantly different. It is interesting to note that the free-surface and rigid-lid currents are still quite different when averaged over three complete seiche cycles (42 hours).

The instantaneous currents computed by the rigid-lid model are generally weaker than the free-surface currents (see Figures 6.12 to 6.14). The rigid-lid currents indicate a much faster response to the wind and generally agree very well with the results of a steady-state model (Gedney and Lick, 1971).

Since the winds were generally strong during the first day and lighter during the second day, it is of interest to compare the daily averaged free-surface and rigid-lid currents during the two-day period. Daily averaged currents have also been used in studies of long-term, time-dependent dispersion of pollutants in Lake Erie (Lam and Jaquet, 1976). Thus it is important to investigate the differences in long-term averaged currents between the free-surface and the rigid-lid models, particularly in the study of the dispersion of pollutants in a lake. As shown in Figures 6.20 and 6.21, the daily-averaged currents computed by the two models agreed quite well on March 7 but differed considerably on March 8. This can be understood as follows. Although the effects of seiche oscillations were important throughout much of the two-day period, the winds were also quite strong on the first day. Hence, the direct wind-driven effect on the currents was dominant over the effects of seiche oscillations. On March 8, the winds decreased significantly and the effects of sieche oscillations became relatively more important. The rigid-lid currents thus differed considerably from the free-surface currents even when averaged over 24 hours. Although not presented here, it can be shown that the differences between the daily-averaged free-surface and rigid-lid currents was more pronounced at depths than near the free surface.

Due to the observed differences in long-term time-averaged currents as computed by the free-surface and the rigid-lid models, applications of the two models of studies of long-term dispersion of substances in a lake may cause appreciable differences in the results. In addition, the strong transient currents due to seiche oscillations as predicted by the free-surface model essentially lead to larger mixing of substances than do the rigid-lid currents. Recently, Sheng and Lick (1977a,b) studied the time-dependent flow and dispersion of sediments in the Western Basin of Lake Erie with a two-dimensional (one vertical and one horizontal) free-surface numerical model and demonstrated that both the transient currents and the short-period waves may cause large shear stresses at the lake bottom, and hence significant resuspension of sediments from the bottom. Due to the fact that the

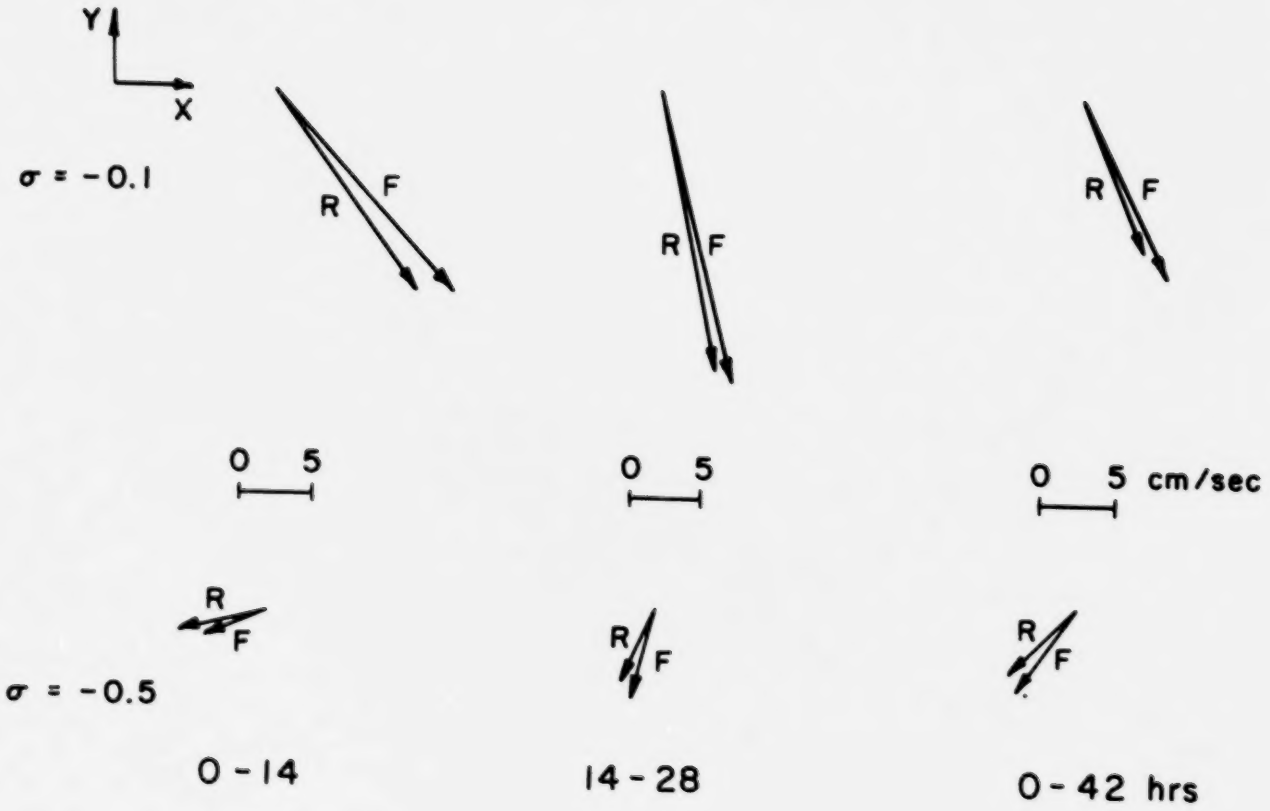

Figure 6.18. Time-averaged currents over 3 14-hour periods and the 42-hour period starting 0000 3/7/76 at Station 1 (near Toledo).

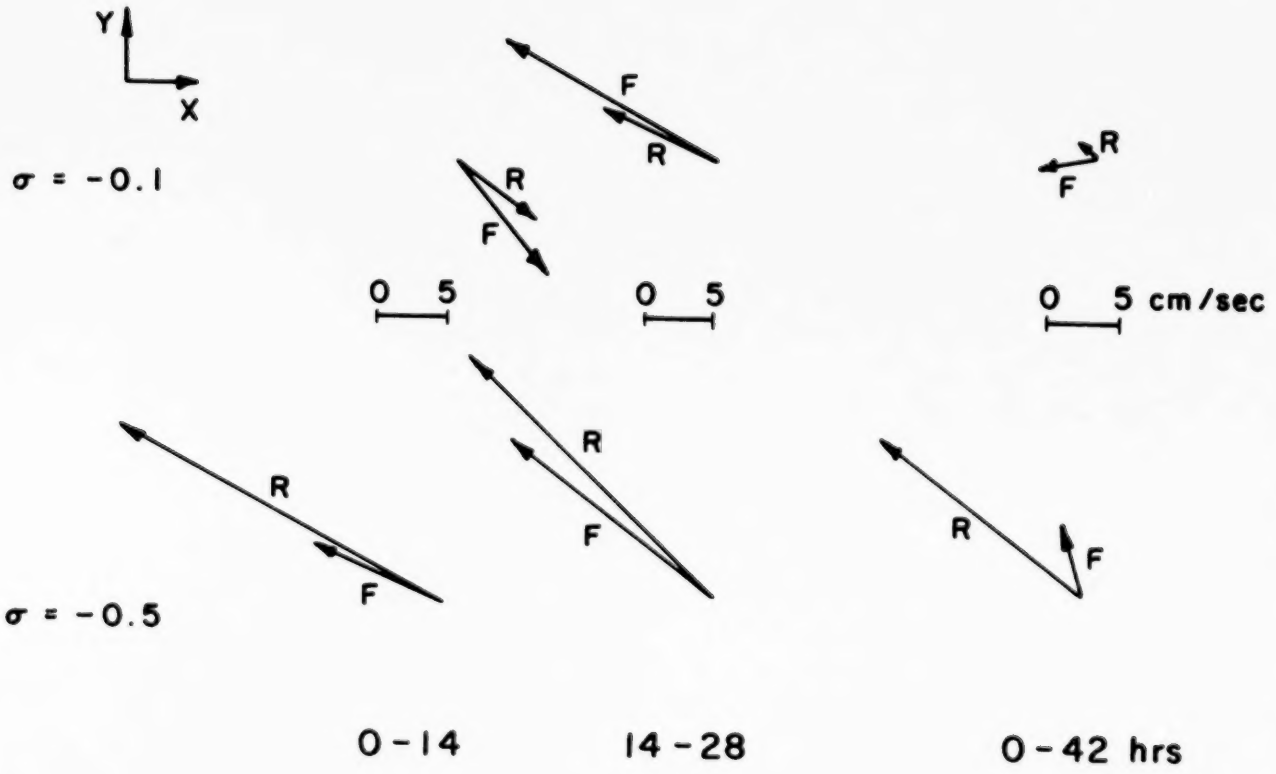

Figure 6.19. Time-averaged currents over 3 14-hour periods and the 42-hour period starting 0000 3/7/76 at Station 2 (near Point Pelee).

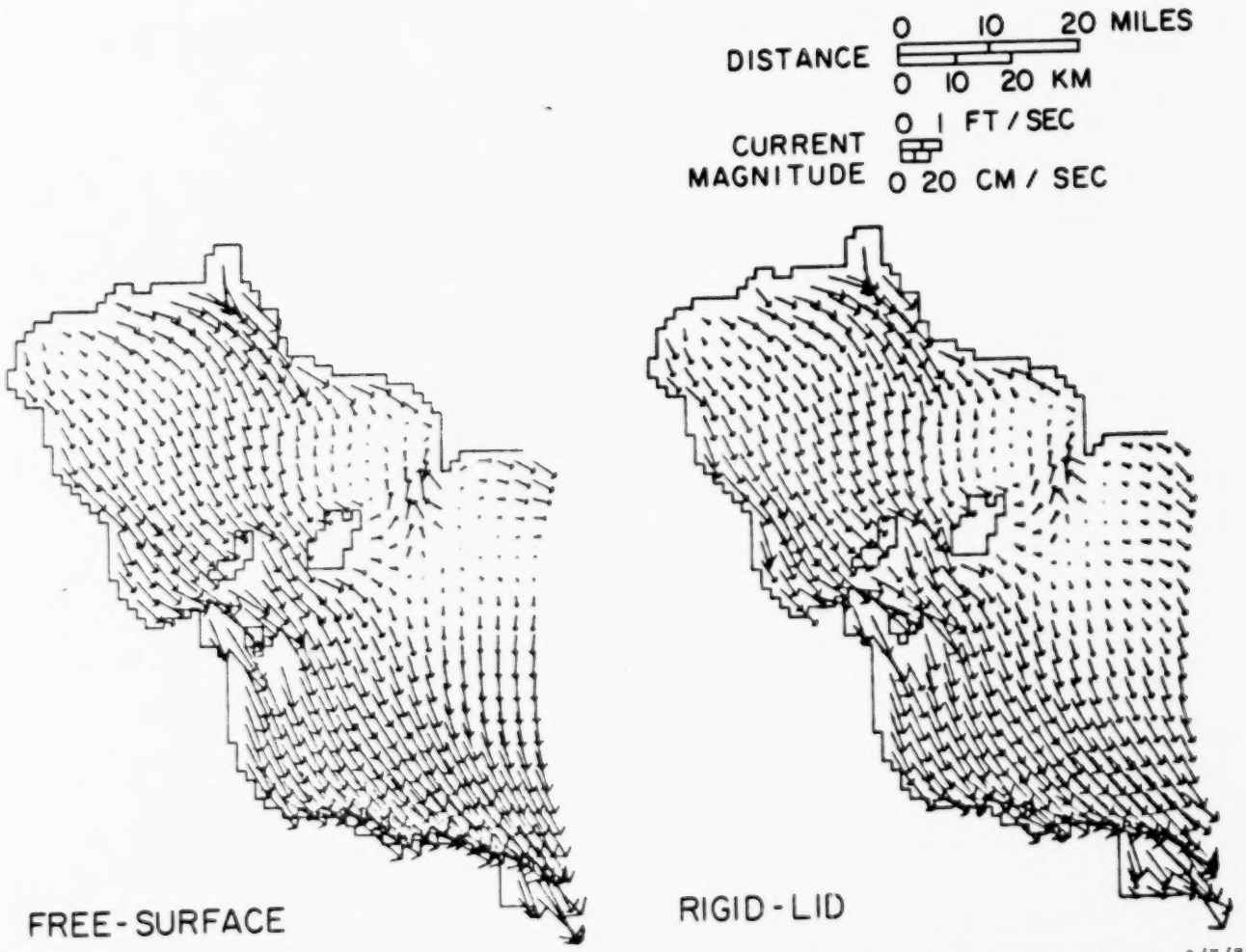

Figure 6.20 Daily-averaged horizontal velocities at a constant 0.1 depth from surface face on 3/7/76.

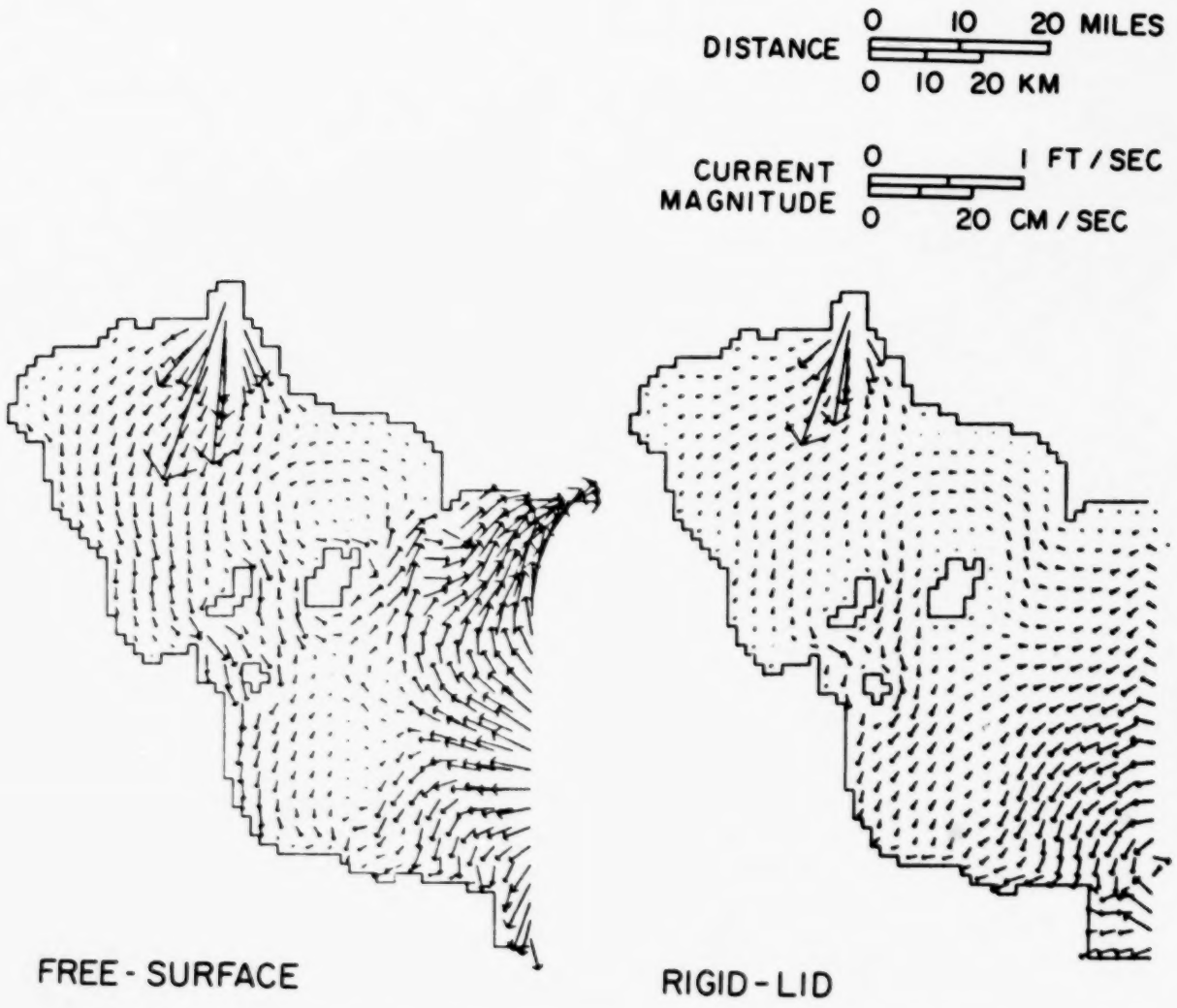

Figure 6.21 Daily-averaged horizontal velocities at a constant 0.1 depth from surface on 3/8/76.

currents as predicted by the rigid-lid model are generally smaller than those predicted by the free-surface model, the use of a rigid-lid model would generally result in smaller bottom shear stresses and less sediment resuspended from the bottom.

Effect of Non-Linear Inertia and Horizontal Turbulence

In Lake Erie under non-stratified conditions, $R_B << 1$ and $E_H << 1$. Hence non-linear inertia and horizontal turbulence can generally be neglected compared to Coriolis and vertical turbulence, respectively. In a numerical study, Sheng (1975) found that the thicknesses of the coastal boundary layers in a non-stratified Lake Erie were on the order of 1 Km or less. Hence the non-linear inertia and horizontal turbulence terms, which are important within the coastal boundary layers, can be neglected if a horizontal numerical grid larger than 1 Km is used. In the present study with a 1.6-Km grid, the time-dependent currents in the Western Basin were computed with and without the non-linear inertia and horizontal turbulence terms in the governing equations and the results compared for up to 12 hours. For both the constant wind and the variable wind cases, the horizontal currents computed with and without these terms were almost identical throughout the entire basin. Hence the non-linear inertia and horizontal turbulence terms were neglected during subsequent calculations, resulting in significant saving of computer time. However, in a stratified lake, thermal convection generally has a strong influence on the temperature field, which in turn significantly influences the flow field, and hence the nonlinear inertia (or convective) terms must be retained.

REFERENCES

Bennett, J.R., 1977: A Three-Dimensional Model of Lake Ontario's Summer Circulation, I. Comparison with Observations, J. Phys. Oceanogr., 7, 591-601.

Berdahl, P., 1971: Oceanic Rossby Waves: A Numerical Rigid-Lid Model. Rept. ITD - 4500, UC-34, Lasrence Radiation Lab., U. of Calif., Livermore.

Cheng, R.T., T.M. Powell and T.M. Dillon, 1976: Numerical Models of Wind-Driven Circulation in Lakes, Appl. Math. Modelling, 1, 141-159.

Crowley, W.P., 1969: A Numerical Model for Viscous Free Surface Barotropic Wind-Driven Ocean Circulation, J. Comp. Phys., 5.

Crowley, W.P., 1970: A Numerical Model for Viscous Non-Divergent, Barotropic, Wind-Driven, Ocean Circulation, J. Comp. Phys., 6.

Donaldson, D.duP., 1973: Atmospheric Turbulence and the Dispersal of Atmospheric Pollutants, AMS Workshop of Micrometeorology, Boston, 313-390, Also EPA-R4-73-016a.

Freeman, M.J., A.M. Hale and M.B. Danard, 1972: A Modified Sigma Equations Approach to the Numerical Modelling of the Great Lakes Hydrodynamics, J. Geo. Res., 77, 1050-1060.

Gedney, R.T. and W. Lick, 1971: Wind-Driven Currents in Lake Eric, J. Geo. Res., 77, No. 15.

Haq, A., W. Lick, and Y.P. Sheng, 1974: The Time-Dependent Flow in Large Lakes with Application to Lake Erie, Tech. Rept., Earth Sci. Dept., Case Western Reserve Univ., Cleveland, Ohio.

Harlow, F.H., and P.I. Nakayama, 1967: Turbulence Transport Equations, The Physics of Fluids, Vol. 10, No. 11.

Kizlauskaus, A.G. and P.L. Katz, 1973: A Numerical Model for Summer Flows in Lake Michigan, Arch. Meteor. Geophys. Bioklim.

Kolmogorov, A.N., 1942: Equations of Turbulent Motion of an Incompressible Turbulent Fluid, Izv. Akad. Nauk. SSSR Ser. Phys. VI, No. 1-2.

Lam, D.C.L. and J.-M. Jaquet, 1976: Computations of Physical Transport and Regeneration and Phosphorus in Lake Erie, Fall 1970, J. Fish. Res. Bd. Can., 33, 550-563.

Launder, B.E. and D.B. Spalding, 1972: Mathematical Models of Turbulence, Academic Press, New York, N.Y.

Lewellen, W.S., M. Teske, and Y.P. Sheng, 1978: Progress Report on Modeling Tornado Dynamics (An Assessment of the Sensitivity of Model Results to the Turbulence Model), A.R.A.P. Tech. Memo. 78-5.

Lick, W., 1976a: Numerical Models of Lake Currents, U.S. Environmental Protection Agency, Washington, D.C.

Lick, W., 1976b: Numerical Modeling of Lake Currents, Annual Review of Earth and Planetary Sciences, Vol. 4.

Liggett, J.A., 1969: Unsteady Circulation in Shallow, Homogeneous Lakes, J. Hydr. DIV., Proc. ASCE, 95 (HY4), 1273-1288.

Munk, W.H. and E.R. Anderson, 1948: Notes on A Theory of the Thermocline, J. of Mar. Res., 7.

Paul, J. and W. Lick, 1974: A Numerical Model of Thermal Plumes and River Discharges. Proc. 17th Conf. GLR, IAGLR.

Paul, J. and W. Lick, 1979: A Rigid-Lid Lake Circulation Model. U.S. EPA, Washington, D.C.

Phillips, N.A., 1957: A Co-ordinate System Having Some Special Advantages for Numerical Forecasting. J. Meteorol., 14.

Platzman, G.W., 1963: The Dynamic Prediction of Wind Tides on Lake Erie, Meteorology Monograph, 4.

Richtmeyer, R.D. and K.W. Morton, 1967: 'Difference Methods for Initial Value Problems', John Wiley, N.Y.

Roache, P.T., 1972: 'Computational Fluid Dynamics', Hermosa Pub., Albuqureque, N.M.

Sheng, Y.P., 1975: Wind-Driven Currents and Dispersion of Contaminants in the Near-Shore of Large Lakes. Ph.D. thesis, School of Engrg., Case Western Reserve Univ., Also as Rept. H-75-1, U.S. Army Engrg. Waterways Exp. Stn., Vicksburg, Miss. (NTIS AD-A017694).

Sheng, Y.P. and W. Lick, 1976: Currents and Contaminant Dispersion in the Near-Shore Regions and Modification by Jetport. J. Great Lakes Res. 2, 402-414.

Sheng, Y.P. and W. Lick, 1977a: Numerical Modelling of the Time-Dependent Flow and Dispersion of Sediments in a Shallow Lake, presented at the 1977 AGU Midwest Meeting, Purdue Univ., Sept. 26-28.

Sheng, Y.P. and W. Lick, 1977b: A Three-Dimensional Numerical Model for the Time-Dependent Flow and Dispersion of Sediments in the Western Basin of Lake Erie, presented at the 1977 AGU Fall Meeting, San Francisco, Dec. 5-9, Transaction AGU, 58, 12.

Sheng, Y.P., W. Lick, R. Gedney and F. Molls, 1978: A Comparison of a Free-Surface and a Rigid-Lid Model, J. Phys. Oceanogr., 8.

Simons, T.J., 1972: Development of Numerical Models for Lake Ontario. Proc. 15th Conf. GLR, IAGLR, 655-672.

Simons, T.J., 1974: Verification of Numerical Models of Lake Ontario Part I: Circulation in Spring, Early Summer, J. Phys. Oceanogr., 5, 98-110.

Sundaram, T.R. and R.G. Rehm, 1970: Formation and Maintenance of Thermoclinics in Stratified Lakes Including the Effects of Power Plant Thermal Discharges, AIAA Paper No. 70-238.

Wilson, B.W., 1960: Note on Surface Wind Stress Over Water at Low and High Speeds, J. Geo. Res., 65, 3377-3382.

APPENDIX A

DERIVATION OF THE VERTICALLY STRETCHED EQUATIONS

In order to incorporate variable bottom topography into a general lake circulation model, vertically stretched coordinates can be used. This procedure maps the variable depth basin to a constant depth one (with modified equations) and results in an equal number of evenly spaced vertical grid points in both the shallow and deeper parts of the basin.

The coordinate system is transformed from x,y,z, to α,β,σ, where $\alpha=x$, $\beta = y$, and $\sigma = z/h(x,y)$. Hence it can be shown that (A-1)

$$\left(\frac{\partial\sigma}{\partial x} \, , \, \frac{\partial\sigma}{\partial y}\right) = -\frac{\sigma}{h}\left(\frac{\partial h}{\partial\alpha} \, , \, \frac{\partial h}{\partial\beta}\right) \tag{A-2}$$

$$\left(\frac{\partial^2\sigma}{\partial x^2} \, , \, \frac{\partial^2\sigma}{\partial y^2}\right) = \left(-\frac{\sigma}{h}\frac{\partial^2 h}{\partial x^2} + \frac{2\sigma}{h^2}\left(\frac{\partial h}{\partial x}\right)^2 \quad , \quad -\frac{\sigma}{h}\frac{\partial^2 h}{\partial\beta^2} + \frac{2\sigma}{h^2}\frac{\partial h}{\partial\beta}\right) \tag{A-3}$$

$$\frac{\partial}{\partial x} = \frac{\partial}{\partial\alpha} - \frac{\sigma}{h}\frac{\partial h}{\partial\alpha}\frac{\partial}{\partial\sigma} \tag{A-4}$$

$$\frac{\partial}{\partial y} = \frac{\partial}{\partial\beta} - \frac{\sigma}{h}\frac{\partial h}{\partial\beta}\frac{\partial}{\partial\sigma} \tag{A-5}$$

$$\frac{\partial}{\partial z} = \frac{1}{h}\frac{\partial}{\partial\sigma} \tag{A-6}$$

and

$$\frac{\partial^2}{\partial x^2} = \frac{\partial^2}{\partial\alpha^2} + 2\frac{\partial\sigma}{\partial x}\frac{\partial^2}{\partial\alpha\partial\sigma} + \frac{\partial^2\sigma}{\partial x^2}\frac{\partial}{\partial\sigma} + \left(\frac{\partial\sigma}{\partial x}\right)^2\frac{\partial^2}{\partial\sigma^2} \tag{A-7}$$

$$\frac{\partial}{\partial y^2} = \frac{\partial^2}{\partial\beta^2} + 2\frac{\partial\sigma}{\partial y}\frac{\partial^2}{\partial\beta\partial\sigma} + \frac{\partial^2\sigma}{\partial y^2}\frac{\partial}{\partial\sigma} + \left(\frac{\partial\sigma}{\partial y}\right)^2\frac{\partial^2}{\partial\sigma^2} \tag{A-8}$$

$$\frac{\partial^2}{\partial z^2} = \frac{1}{h^2} \frac{\partial^2}{\partial \sigma^2} \tag{A-9}$$

Define

$$u = \frac{1}{R_B} \frac{dx}{dt} = \frac{1}{R_B} \frac{d\alpha}{dt} \tag{A-10}$$

$$v = \frac{1}{R_B} \frac{dy}{dt} = \frac{1}{R_B} \frac{d\beta}{dt} \tag{A-11}$$

$$\omega = \frac{1}{R_B} \frac{d\sigma}{dt} \tag{A-12}$$

where ω is related to the vertical velocity w by:

$$w = \omega h + \sigma \left(u \frac{\partial h}{\partial x} + v \frac{\partial h}{\partial y} \right) \tag{A-13}$$

The expression

$$\frac{\partial A}{\partial t} + R_B \left(\frac{\partial uA}{\partial x} + \frac{\partial vA}{\partial y} + \frac{\partial wA}{\partial z} \right) \tag{A-14}$$

where A is the appropriate dependent variable (1 for the continuity equation u, v, w for the three momentum equations, and T for the energy equation), can be transformed into the following form:

$$\frac{\partial A}{\partial t} + R_B \left[\frac{\partial}{\partial \alpha} (uA) - \frac{\sigma}{h} \frac{\partial h}{\partial \sigma} \frac{\partial}{\partial \sigma} (uA) + \frac{\partial}{\partial \beta} (vA) - \frac{\sigma}{h} \frac{\partial h}{\partial \beta} \frac{\partial}{\partial \sigma} (vA) + \frac{1}{h} \frac{\partial}{\partial \sigma} (wA) \right] \tag{A-15}$$

Substituting (A-13) into (A-15), we get

$$\frac{1}{h} \frac{\partial hA}{\partial t} + R_B \left[\frac{\partial (huA)}{\partial \alpha} + \frac{\partial (hvA)}{\partial \beta} + h \frac{\partial (\omega A)}{\partial \sigma} \right] \tag{A-16}$$

The horizontal turbulence terms

$$E_H \left(\frac{\partial^2 A}{\partial x^2} + \frac{\partial^2 A}{\partial y^2} \right) \tag{A-17}$$

where A is u, v, or T, can be transformed into the following form:

$$\frac{E_H}{h}\left[\frac{\partial}{\partial\alpha}\left(h\frac{\partial A}{\partial\alpha}\right)+\frac{\partial}{\partial\beta}\left(h\frac{\partial A}{\partial\beta}\right)-\frac{\partial h}{\partial\alpha}\frac{\partial}{\partial\sigma}\left(\sigma\frac{\partial A}{\partial\alpha}\right)-\frac{\partial h}{\partial\beta}\frac{\partial}{\partial\sigma}\left(\sigma\frac{\partial A}{\partial\beta}\right)-\right.$$
$$\left.\sigma\frac{\partial}{\partial\alpha}\left(\frac{\partial h}{\partial\alpha}\frac{\partial A}{\partial\sigma}\right)-\sigma\frac{\partial}{\partial\beta}\left(\frac{\partial h}{\partial\beta}\frac{\partial A}{\partial\sigma}\right)+\frac{1}{h}\left(\left(\frac{\partial h}{\partial\alpha}\right)^2+\left(\frac{\partial h}{\partial\beta}\right)^2\right)\frac{\partial}{\partial\sigma}\left(\sigma^2\frac{\partial A}{\partial\sigma}\right)\right] \tag{A-18}$$

The first two terms in (A-18) are generally much larger than the other terms which contain bottom slopes or their products and hence are of higher order in a basin with H/L<<1. However, these higher order terms may be comparable to the leading terms in regions of sharp bottom slopes.

The vertical turbulence term

$$E_v\frac{\partial}{\partial z}\left(A_v\frac{\partial A}{\partial z}\right) \tag{A-19}$$

can be transformed into

$$\frac{E_v}{h^2}\frac{\partial}{\partial\sigma}\left(A_v\frac{\partial A}{\partial\sigma}\right) \tag{A-20}$$

The horizontal turbulence terms in the vertically integrated equations in an x,y,z system are

$$E_H\int_{-h}^{o}\left(\frac{\partial^2 A}{\partial x^2}+\frac{\partial^2 A}{\partial y^2}\right)dz \tag{A-21}$$

where A is u or v.

The corresponding expression in the transformed α,β,σ system can be obtained by vertically integrating Eq. (A-18) from $\sigma = -1$ to $\sigma = 0$ and is:

$$E_H\left(\frac{\partial^2\tilde{A}}{\partial\alpha^2}+\frac{\partial^2\tilde{A}}{\partial\beta^2}\right)-\frac{E_H}{h}\left[\left(\frac{\partial h}{\partial\alpha}\right)^2+\left(\frac{\partial h}{\partial\beta}\right)^2\right]\left(\frac{\partial A}{\partial\sigma}\right)_{\sigma=-1} \tag{A-22}$$

where $\tilde{A}$ is defined as

$$\tilde{A} = h\int_{-1}^{o}A\,d\sigma \tag{A-23}$$

The transformed equations are as shown in Eqs. (2.20) through (2.24).

APPENDIX B

AN IMPLICIT SCHEME

The heat equation is here considered in non-dimensional form:

$$\frac{\partial u}{\partial t} = \frac{E_v}{h^2} \frac{\partial^2 u}{\partial \sigma^2} \tag{B-1}$$

The forward-time central-space (FTCS) scheme solves Eq. (B-1) by means of the following finite-difference equation:

$$u_K^{n+1} = u_K^n + \alpha(u_{K+1}^n = 2u_K^n + u_{K-1}^n)\ \Delta t \tag{B-2}$$

where $\alpha = E_v/(h\Delta\sigma)^2$, n and n+1 are indices representing previous and present time levels, K indicates the vertical level, and t is the non-dimensional time step. Numerical stability requires the following criterion to be satisfied:

$$\Delta t \leq \frac{1}{2\alpha} \tag{B-3}$$

This condition is very restrictive for a shallow lake such as Lake Erie. To alleviate this problem, several schemes can be used. The Du-Fort Frankel scheme uses the following form:

$$u_K^{n+1} = u_K^{n-1} + \alpha(u_{K+1}^n - u_K^{n+1} - u_K^{n-1} + u_{K-1}^n)\ \Delta t \tag{B-4}$$

Hence

$$(1 + \alpha\Delta t)u_K^{n+1} = (1 - \alpha\Delta t)u_K^{n-1} + \alpha(u_{K+1}^n + u_{K-1}^n)\ \Delta t \tag{B-5}$$

It can be shown that the Du-Fort Frankel scheme is unconditionally stable but gives oscillatory results due to time-splitting (Roache, 1972). The Hopskotch scheme is also unconditionally stable and uses the following forms:

Odd n, even K and even n, odd K;

$$u_K^{n+1} = u_K^n + \alpha\Delta t\ (u_{K+1}^n - 2u_K^n + u_{K-1}^n) \tag{B-6}$$

Odd n, odd K and even n, even K:

$$u_K^{n+1} = u_K^n + \alpha\Delta t \ (u_{K+1}^{n+1} - 2u_K^{n+1} + u_{K-1}^{n+1}) \qquad \text{(B-7)}$$

Both the Du-Fort Frankel and the Hopskotch schemes were used to solve Eq. (B-1) and the results contained non-physical oscillations during the transient stage, although both schemes converged to the same steady state.

Sheng (1975) modified the Du-Fort Frankel scheme and applied the following form to compute the dispersion of contaminants in the near-shore regions of Lake Erie:

$$u_K^{n+1} = u_K^n + \alpha\Delta t \ (u_{K+1}^{n} - u_K^{n+1} - u_K^{n-1} + u_{K-1}^{n}) \qquad \text{(B-8)}$$

Relatively large numerical time steps up to 1 hour were used in the calculation with a horizontal spatial grid of 0.4 Km.

In order to have a numerically stable scheme and also alleviate the non-physical oscillations, a completely implicit scheme can be used:

$$u_K^{n+1} = u_K^n + \alpha\Delta t \ (u_{K+1}^{n+1} - 2u_K^{n+1} + u_{K-1}^{n+1}) \qquad \text{(B-9)}$$

The following boundary conditions were used:

$$u = 0 \text{ at } \sigma = -1 \qquad \text{(B-10)}$$

$$\frac{\partial u}{\partial \sigma} = \frac{\tau_x^w}{E_v} \text{ at } \sigma = 0 \qquad \text{(B-11)}$$